An F0-based genetic assay in adult zebrafish for discovering modifier genes of an inherited cardiomyopathy

Yonghe Ding[1,2]*, Mingmin Wang[1,2,3,4]*, Haisong Bu[1,2,5], Jiarong Li[1,2,6], Xueying Lin[1,2], Xiaolei Xu[1,2‡]

[1]Department of Biochemistry and Molecular Biology, Mayo Clinic, Rochester, Minnesota, USA

[2]Department of Cardiovascular Medicine, Mayo Clinic, Rochester, Minnesota, USA

[3]Dongzhimen Hospital, Beijing University of Chinese Medicine, Beijing, China

[4]Current address: Zhejiang Traditional Chinese Medicine Hospital, Hangzhou, China

[5]Department of Cardiothoracic Surgery, Xiangya Hospital, Central South University, Changsha, China.

[6]Department of Cardiovascular Surgery, The Second Xiangya Hospital of Central South University, Changsha, China

*These authors contributed equally to this work.

‡**Correspondence:** Xiaolei Xu, PhD, Department of Biochemistry and Molecular Biology, Department of Cardiovascular Medicine, Mayo Clinic, 200 First Street SW, Rochester, Minnesota, 55905, USA. Phone: +1(507)284-0685; E-mail: xu.xiaolei@mayo.edu.

© 2022. Published by The Company of Biologists Ltd.
This is an Open Access article distributed under the terms of the Creative Commons Attribution License (http://creativecommons.org/licenses/by/4.0), which permits unrestricted use, distribution and reproduction in any medium provided that the original work is properly attributed.

Disease Models & Mechanisms • DMM • Accepted manuscript

ABSTRACT

Modifier genes contribute significantly to our understanding of pathophysiology in human diseases; however, effective approaches to identify modifier genes have been lacking. Here, we aim to develop a rapid F0-based genetic assay in adult zebrafish using the *bag3* gene knockout (*bag3*$^{e2/e2}$) cardiomyopathy model as a paradigm. First, utilizing a classic genetic breeding approach, we identified *dnajb6b* as a deleterious modifier gene for *bag3* cardiomyopathy. Next, we established an F0-based genetic assay in adult zebrafish through injection of predicted microhomology-mediated end joining (MMEJ)-inducing single guide RNA/Cas9 protein complex. We showed that effective gene knockdown is maintained in F0 adult fish, enabling recapitulation of both salutary modifying effects of the *mtor* haploinsufficiency and deleterious modifying effects of the *dnajb6b* gene on *bag3* cardiomyopathy. We finally deployed the F0-based genetic assay to screen differentially expressed genes in the *bag3* cardiomyopathy model. As a result, *myh9b* was identified as a novel modifier gene for *bag3* cardiomyopathy. Together, these data prove the feasibility of an F0 adult zebrafish-based genetic assay that can be effectively used to discover modifier genes for an inherited cardiomyopathy model.

INTRODUCTION

Phenotypic variation occurs in many inherited human diseases, and as a result, has made it difficult to identify specific mechanisms and potential therapeutics. For example, patients with identical cardiomyopathy-causing mutations, such as mutations in *RBM20, TNNI3,* or *BAG3* could manifest highly variable disease onset and severity (Arad et al., 2002; Hwang et al., 2017; Norton et al., 2011; Pantou et al., 2018). Reasons for phenotypic variation are difficult to distinguish, as differences could result from combinatory interactions among several causative genes (Deacon et al., 2019; Gifford et al., 2019) or co-existence of a causative gene and a

Disease Models & Mechanisms • DMM • Accepted manuscript

modifier gene(s), i.e., genes that either exacerbate or attenuate disease progression, but may not cause the disease per se (Hershberger et al., 2013; Sen-Chowdhry et al., 2010). Genomic technology such as genome-wide association studies (GWASs) in humans (Dorn, 2011; Mouton et al., 2016; Su et al., 2014; Visscher et al., 2012) and quantitative trait locus analyses in rodents (Daw et al., 2008; Le Corvoisier et al., 2003; Suzuki et al., 2002; Wheeler et al., 2005; Wheeler et al., 2009) has previously been applied to search for modifier genes. However, these statistics-based methods often end up with large genomic loci that cover many candidate genes, making it difficult to establish precise genotype-phenotype relationship. In order to identify more specific genetic relationships, experimental assessment requires multiple-generations of breeding and large number of mutant animals (Gifford et al., 2019), thus the demand for colony management efforts can be prohibitively high and a more efficient genetic assay to facilitate the discovery of modifier genes is highly desirable.

Because of its higher throughput than most other vertebrate models, zebrafish possess unique advantages for developing new methods that enable the discovery of modifying genes. Building on an efficient Gene-Break Transposon (GBT)-based insertional mutagenesis platform, a forward genetic screen-based method has been recently established to identify modifier genes for anthracycline - induced cardiotoxicity (AIC) (Ding et al., 2013; Ding et al., 2016; Ding et al., 2011). Deleterious modifiers such as *dnajb6b* and *sorbs2b* as well as salutary modifiers like *rxraa* and *mtor* were identified (Ding et al., 2019; Ding et al., 2016; Ding et al., 2020; Ma et al., 2020). The obvious advantages of this novel approach are that the identity of modifier genes can be unambiguously uncovered, and that the methods can be easily scaled to the genome for systematic identification of AIC modifiers. However, it remains unverified whether this new approach based on chemically induced AIC model is extendable to an inherited cardiomyopathy model, which still requires the generation of a large number of double mutants.

Disease Models & Mechanisms • DMM • Accepted manuscript

The advent of the CRISPR/Cas9–based genome editing technology has created new opportunities for efficient genetic studies. Several recent studies demonstrated the feasibility of genetic analysis in F0 animals in different species, eliminating the need of generating large number of stable mutant lines (Ata et al., 2018; Kroll et al., 2021; Wu et al., 2018). With these new genetic tools, it is possible to rapidly screen 50 cardiomyocyte transcriptional regulators at one time. This breakthrough has led to the discovery of *zbtb16a* as a new gene for cardiac development (Wu et al., 2018). To ensure high knockout (KO) efficiency in F0, four CRISPR/Cas9 ribonucleoprotein complexes targeting each gene of interest were co-injected. While the majority of these efforts is based on the CRISPR/Cas9 platform that induces non-homologous end joining (NHEJ), a microhomology-mediated end-joining (MMEJ)-based genome technology has been recently adapted in zebrafish embryos for faithfully recapitulating loss-of-function phenotypes in F0 animals (Ata et al., 2018; Martinez-Galvez et al., 2021). Different from NHEJ, which often leads to unpredictable DNA repair outcomes including those do not shift the reading frame, injection of predicted MMEJ-inducing single guide (sgRNA) incurs more precise and homogenous genetic lesion while simultaneously maintains high level of knockout (KO) efficiency (Ata et al., 2018; Martinez-Galvez et al., 2021; Shen et al., 2018). As a consequence, injection of a single predicted MMEJ-inducing sgRNA was typically sufficient to incur predictable biallelic mutations in the F0 animals (Martinez-Galvez et al., 2021).

Prompted by the success of F0-based genetic assay in zebrafish embryos, here, we explored whether this assay can achieve the same success in adult zebrafish. We decided to develop this assay by using *bag3*$^{e2/e2}$ KO fish, one of the first inherited cardiomyopathy models in adult zebrafish (Ding et al., 2019). *BAG3* is a defined causative gene for human dilated cardiomyopathy (DCM), which encodes a co-chaperone protein that plays an important role in regulating protein quality control and autophagic proteostasis (Myers et al., 2018). Like many other inherited cardiomyopathy diseases, significant phenotypic variation has been observed

Disease Models & Mechanisms • DMM • Accepted manuscript

among affected humans who share the same mutations in the *BAG3* gene (Dominguez et al., 2018; Norton et al., 2011). To set up such an F0-based assay, we firstly utilized classic genetic breeding approach to identify common modifier genes suggested from the acquired AIC model. We found that the predicted MMEJ-based F0 genetic assay is able to rapidly recapitulate the modifying effects of the *bag3*$^{e2/e2}$ stable mutants. To test the robustness of the F0-based genetic assay, we analyzed 8 differentially expressed (DE) genes resultant from a transcriptome study of *bag3*$^{e2/e2}$, and identified *myh9b* as a new modifier gene for *bag3* cardiomyopathy. Together, our data proved the feasibility of utilizing a F0-based genetic assay for discovering modifier genes in a cardiac disease model.

RESULTS

dnajb6b, an anthracycline-induced cardiomyopathy (AIC) modifier, is also a modifier gene for *bag3* cardiomyopathy.

Because *bag3* cardiomyopathy shares common phenotypes such as heart remodeling and cardiac dysfunction with anthracycline-induced cardiomyopathy (AIC), we reasoned that some genetic modifiers of AIC identified from the forward genetic approach would also exert similar modifying effects on *bag3* cardiomyopathy. To test this possibility, we took a classic genetic approach and crossed gene-break transposon (*GBT) 002/sorbs2b, GBT136/ano5a, GBT411/dnajb6b*, and *GBT419/rxraa,* four modifying mutants for AIC, into the *bag3* cardiomyopathy model (Ding et al., 2016; Ding et al., 2020; Ma et al., 2020). For clarity, these 4 modifying mutants will be subsequently referred to the disrupted genes: *sorbs2b*, *ano5a, dnajb6b* and *rxraa*, respectively. To maximize sensitivity of detecting modifying effects, we generated stable double homozygous mutants and quantified cardiac pump functions in adult fish at 6 months non-invasively using the High-Frequency Echocardiography (HFE).

Disease Models & Mechanisms • DMM • Accepted manuscript

Compared to the *bag3*$^{e2/e2}$ mutant alone, we did not detect any significant changes of cardiac function in the *bag3*$^{e2/e2}$*;sorb2b*$^{-/-}$, *bag3*$^{e2/e2}$*; ano5a*$^{-/-}$ or *bag3*$^{e2/e2}$*; rxraa*$^{-/-}$ double homozygous mutant lines (Fig. 1A and 1B). By contrast, the *bag3*$^{e2/e2}$*;dnajb6b*$^{-/-}$ fish failed to survive to adulthood and all died within 5 weeks (Fig. 1C). Detailed studies of the *bag3*$^{e2/e2}$*;dnajb6b*$^{-/-}$ double mutant fish during embryonic stages uncovered significantly reduced cardiac function and increased ventricular chamber size starting at 6 days post-fertilization (dpf) (Fig. 1D-F). Other phenotypes include missing swim bladder and an unusually protruding jaw (Supplemental Fig. 1). These data suggested that *GBT411/dnajb6b,* an AIC modifying mutant, also exerts deleterious modifying effects on the *bag3*$^{e2/e2}$ cardiomyopathy.

We then assessed the genetic interaction when these two genes are partially disrupted. Similar to the juvenile lethal phenotypes in the *bag3*$^{e2/e2}$*;dnajb6b*$^{-/-}$ mutants, *bag3*$^{e2/e2}$*;dnajb6b*$^{+/-}$ double mutant fish died within 6 weeks (Supplemental Fig. 2), underscoring a strong genetic interaction between the *bag3* and *dnajb6b* genes. By contrast, up to 20% of *bag3*$^{e2/+}$*; dnajb6b*$^{-/-}$ double mutant fish were viable for at least 12 weeks (Fig. 2A), enabling characterization of adult phenotypes incurred by concomitant deficiency of *bag3* and *dnajb6b* genes. Significantly declined cardiac function, accompanied by enlarged ventricular surface area (VSA) was noted in the *bag3*$^{e2/+}$*; dnajb6b*$^{-/-}$ double mutant fish at 3 months (Fig. 2B, 2C). The *bag3*$^{e2/+}$*; dnajb6b*$^{-/-}$ double mutant fish at 3 months displayed a similar protruding jaw phenotype to the *bag3*$^{e2/e2}$*; dnajb6b*$^{-/-}$ double homozygous embryos at 6 dpf (Supplemental Fig. 3). In the *dnajb6b*$^{-/-}$ mutant, we also noted mild lipid accumulation on the surface of ventricular chamber and elevated protein ubiquitination, both of which are exaggerated in the hearts of *bag3*$^{e2/+}$*; dnajb6b*$^{-/-}$ double mutant (Fig. 2D, 2E). In addition, abnormal mitochondria swelling and myofibril loss defects were also noted in the hearts of *bag3*$^{e2/+}$*; dnajb6b*$^{-/-}$ double mutants through transmission electron microscopy (TEM) analysis, but not single mutants (Fig. 2F). Together, these data confirmed a genetic interaction between the *dnajb6b* and *bag3* genes in cardiomyopathy.

Disease Models & Mechanisms • DMM • Accepted manuscript

Moreover, our data suggested functions of *bag3-dnajb6b* co-deficiency in regulating lipid metabolism and proteostasis, two pathological events that are observed in cardiomyopathy (Goldberg et al., 2018; Henning and Brundel, 2017; Wende and Abel, 2010).

Mouse Dnajb6(S), a predominantly somite-expressed short isoform of Dnajb6, has been shown to directly bind Bag3 protein in the skeletal muscle (Sarparanta et al., 2012). The *GBT411/dnajb6b* mutant harbors an insertion that is located after the exons of the short isoform and before the exons of the long isoform, thus specifically disrupts DNAJB6(L), a cardiac-enriched long isoform of DNAJB6 (Ding et al., 2016). We thus enquired whether DNAJB6(L) also binds the BAG3 protein. Using an *in vitro* protein pulldown assay in HEK293 cells, we confirmed the binding of human DNAJB6(S) with human BAG3, and further noted physical interaction between DNAJB6(L) and BAG3 as well (Supplemental Fig. 4A). Moreover, we noted that BAG3 and zebrafish Dnajb6b proteins are co-localized within the sarcomere, as reflected by the human BAG3-EGFP fusion protein and the RFP reporter in the *GBT411/dnajb6b* line, respectively (Supplemental Fig. 4B). Together, both our biochemical and co-localization studies supported a genetic interaction between the *dnajb6b* and *bag3* genes in a zebrafish heart.

Injection of a predicted MMEJ-inducing sgRNAs recapitulated salutary modifying effects of *mtor* and deleterious modifying effects of *dnajb6b* on *bag3* cardiomyopathy in F0 adult zebrafish.

To accelerate the identification of modifiers, we enquired whether the predicted MMEJ-based F0 assays can be used in adult models. We initially tested the *tyrosinase* (*tyr*) gene, since loss-of-function of *tyr* manifests a loss-of-melanophore phenotype that is easily scored non-invasively (Ata et al., 2018). Indeed, we found embryos injected with a high dose of the predicted MMEJ-inducing *tyr* sgRNA at 5 µM (Ata et al., 2018) exhibited near-complete loss of pigmentation at 3

Disease Models & Mechanisms • DMM • Accepted manuscript

dpf. At 3 months, they also manifested near-complete loss of pigmentation (Supplemental Fig. 5A), with a KO score maintained at ~85% from tail fin analysis (Supplemental Fig. 5B and 5C). In contrast, when a low dose of the predicted MMEJ-inducing *tyr* sgRNA at 1 µM was used, lower KO scores were detected, concurrent with an increase in pigmentation (Supplemental Fig. 5 and 5B). Thus, different doses of the injected *tyr* sgRNA correlate with the level of KO score, as well as the severity of pigmentation phenotype. In addition, the KO scores between heart and tail fin, or kidney and tail fin were highly correlated (R^2=0.94 and 0.96, respectively) (Supplemental Fig. 5C), suggesting that the tail fin can be used as a surrogate for measuring genetic deficiency in internal organs. Together, this pilot analysis of an predicted MMEJ-inducing *tyr* sgRNA strongly suggested the feasibility of rapid genotype-phenotype correlation in F0 adult zebrafish.

To confirm whether predicted MMEJ-based genome editing technology is faithful for assessing genetic interactions in F0 adult fish, we decided to target the *mtor* gene because *mtor* haploinsufficiency was recently reported to exert therapeutic effects on *bag3* cardiomyopathy (Ding et al., 2019). We designed a predicted MMEJ-inducing sgRNA using MENTHU (http://genesculpt.org/menthu/) and targeted at the 6th exon of the *mtor* gene. Injection of the sgRNA resulted in a mixture of genetic lesions. As revealed by Tracking Indels by DEcomposition (TIDE) analysis (Brinkman and van Steensel, 2019), the average frame-shift KO score is about 72.9% in injected embryos that maintained at about 67.9% at 3 months, 68.3% of which harbors a 10-nucleotide deletion allele that is predicted to be resulted from microhomology recombination (Fig. 3A, 3B). At the protein level, mTOR expression decreased to about 30% of that in uninjected control (Fig. 3C). We then injected this *mtor* sgRNA (termed as *mtor*$^{e6\text{-}MJ}$) into embryos derived from *bag3*$^{e2/+}$ incrossing, raised up to 6 months, and identified the *mtor*$^{e6\text{-}MJ}$ injected *bag3*$^{e2/e2}$ double mutants (termed as *bag3*$^{e2/e2}$; *mtor*$^{e6\text{-}MJ}$). We noted that EF in the *bag3*$^{e2/e2}$; *mtor*$^{e6\text{-}MJ}$ fish was significantly rescued compared to that in the

Disease Models & Mechanisms • DMM • Accepted manuscript

bag3$^{e2/e2}$ cardiomyopathy model (Fig. 3D). Additionally, we also detected reduction of the elevated protein ubiquitination level, increased trabecular muscle density, and partially restored sarcomeric and mitochondrial swelling defects (Fig. 3E-G). Together, these results demonstrated that the F0-based genetic assay can largely recapitulate salutary modifier effects of the *mtor* haploinsufficiency on *bag3* cardiomyopathy.

Next, we tested whether injection of a predicted *dnajb6b* MMEJ-inducing sgRNA would recapitulate modifying effects between *bag3* and *dnajb6* genes in F0 fish. We designed a predictedMMEJ-inducing sgRNA for the *dnajb6b* gene targeting at exon 6, mimicking the RP2 transposon insertional position in the *GBT411/dnajb6b* mutant (Fig. 4A) (Ding et al., 2013). Injection of the *dnajb6b* sgRNA (termed as *dnajb6b*$^{e6\text{-}MJ}$) resulted in genetic lesions in the targeted locus with an average frame-shift KO score of 68.3% in the F0 embryos. The frame-shift KO score was maintained at about 58.7% in the adult fish, among which 37.5% are the predicted 7-nucleotide deletion alleles presumably resulted from microhomology recombination (Fig. 4A and 4B). At the RNA level, injection of *dnajb6b*$^{e6\text{-}MJ}$ resulted in a reduction of *dnajb6b* transcript to about 19% of the uninjected controls (Fig. 4C), likely due to nonsense-mediated decay. We termed F0 *bag3*$^{e2/e2}$ fish injected with a *dnajb6b* sgRNA as *bag3*$^{e2/e2}$;*dnajb6b*$^{e6\text{-}MJ}$. Compared to uninjected *bag3*$^{e2/e2}$ control, *bag3*$^{e2/e2}$;*dnajb6b*$^{e6\text{-}MJ}$ exhibited significantly reduced fraction shortening (FS) and ejection fraction (EF) (Fig. 4D, 4E). Interestingly, further detailed phenotyping of the F0 *bag3*$^{e2/e2}$*;dnajb6b*$^{e6\text{-}MJ}$ fish identified similar defects to the stable *bag3*$^{e2/+}$*;dnajb6b*$^{-/-}$ double mutants, including increased lipid deposits on the ventricular surface, elevated ubiquitinated protein levels, reduced ventricle trabecular muscle density, abnormally swelled mitochondria, and myofibril loss (Fig. 5). Together, these data suggested that injection of a predicted MMEJ-inducing sgRNA targeting *dnajb6b* recapitulated many, but not all, modifying effects of *GBT411/dnajb6b* on *bag3* cardiomyopathy.

Disease Models & Mechanisms • DMM • Accepted manuscript

Screening 8 differentially expressed (DE) genes via F0 genetic assay identified *myh9b* as a new modifying gene for *bag3* cardiomyopathy.

Encouraged by our success in recapitulating 2 known modifier genes for *bag3* cardiomyopathy, we then enquired whether the predicted MMEJ-based genetic interaction assay in F0 fish is sufficiently robust for discovering new modifier genes. Our previous RNA-seq analysis of heart tissues identified a number of DE genes between the *bag3*$^{e2/e2}$ homozygous fish and WT sibling controls (Ding et al., 2019). We focused on DE genes involved in proteostasis/autophagy, because the BAG3 protein is a proteostatic protein and dysregulated autophagy was noted in both *bag3*$^{e2/e2}$ fish and *Bag3* conditional KO mouse hearts (Fang et al., 2017; Ruparelia et al., 2020). From 27 DE genes previously reported from RNA-seq analysis, 8 DE genes including *myh9b, ulk2a, snrkb, atxn2l, ddit4, pik3r1,rab11fib3,* and *acta1a* were validated experimentally via quantitative reverse transcription polymerase chain reaction (qRT-PCR) analysis (Supplemental Fig. 6). We designed predicted MMEJ-inducing sgRNAs against these genes and obtained >50% KO score in 7 out of 8 genes (Table 1). Individual sgRNAs were then injected into the offsprings of *bag3*$^{e2/+}$ incrossed fish embryos. We found that injection of the sgRNA targeting at the 12th exon of *myh9b* gene exaggerates *bag3* cardiomyopathy, as indicated by significantly reduced EF and enlarged heart chamber size in the *bag3*$^{e2/e2}$*;myh9b*^{MJ} fish compared to uninjected *bag3*$^{e2/e2}$ controls (Fig. 6A-C). In contrast, the other 7 predicted MMEJ-inducing sgRNAs did not cause any significant changes of EF in *bag3*$^{e2/e2}$ fish at 6 months of age (Fig. 6A). Additionally, severe mitochondrial swelling and sarcomeric disarray phenotypes were noted in the *bag3*$^{e2/e2}$*;myh9b*^{MJ} fish by TEM analysis, but were not detected in the *myh9b*^{MJ} alone (Fig. 6D).

To confirm the modifying effects of *myh9b* gene on *bag3* cardiomyopathy, we incrossed the *bag3*$^{e2/+}$*;myh9b*^{MJ} F0 fish with high KO scores to generate stable *bag3*$^{e2/e2}$*;myh9b*$^{e12/+}$ mutants at F1. Different from a mixture of genetic lesions at F0 with averaged KO scores of 67.5% among

Disease Models & Mechanisms • DMM • Accepted manuscript

which 54.8% indels are 8-nucleotdie deletion alleles incurred by predicted microhomology recombination (Fig. 7A and Table 1), the *myh9b* homozygous embryos (*myh9b*$^{e12/e12}$) at F1 derived from F0 incrosses harbored exclusively the 8-nucleotide deletion allele as evidenced by Sanger sequencing (Fig. 7A-B). As expected, KO scores for all *myh9b* F1 heterozygous mutant fish were ~50%. While we failed to recover the *myh9b*$^{e12/e12}$ fish to adulthood, likely because of a recessive lethal phenotype (data not shown), we obtained *myh9b*$^{e12/+}$ which remained viable at the adult stage. We further obtained age-matched groups consisting of *bag3*$^{e2/e2}$, *bag3*$^{e2/e2}$*;myh9b*$^{e12/+}$ and corresponding WT sibling controls from genetic crossing followed by genotyping PCR. While the *bag3*$^{e2/e2}$ cardiomyopathy model manifested reduced EF, the *bag3*$^{e2/e2}$*;myh9b*$^{e12/+}$ double stable mutant fish exhibited further reduced EF compared to WT fish (Fig. 7C). Similar to the *bag3*$^{e2/e2}$*;myh9b*^{MJ} F0 fish, the stable *bag3*$^{e2/e2}$*;myh9b*$^{e12/+}$ mutant F1 fish also displayed more enlarged ventricular chamber size, further reduced autophagy level, and increased sarcomere disarray (Fig. 7D-E. Supplemental Fig.7). Together, these data confirmed *myh9b* as a new modifier gene for *bag3* cardiomyopathy.

DISCUSSION

A predicted MMEJ-inducing sgRNA injection approach in F0 adult zebrafish can be used for discovering genetic modifiers of an inherited cardiomyopathy

Prompted by the predicted MMEJ-induced genome editing technology that has been established recently in zebrafish F0 embryos for functional genomic studies (Ata et al., 2018; Martinez-Galvez et al., 2021), here, we present several pieces of evidence to demonstrate an expanded application of this more precise gene editing technology in F0 adult fish. First, similar to a recent report (Wu et al., 2018), we showed that injection of a predictedMMEJ-inducing sgRNA for the *tyr* gene incurred a loss-of-melanophore phenotype that is sustained from embryonic to adult stage in F0 animals. Second, we demonstrated that modifying effects of

Disease Models & Mechanisms • DMM • Accepted manuscript

dnajb6 and *mtor* on the *bag3* cardiomyopathy can be largely recapitulated in F0 adult fish. Finally, we utilized this F0-based genetic platform to screen differentially expressed (DE) genes and identified *myh9b* as a new genetic modifier for *bag3* cardiomyopathy. This finding was subsequently confirmed by the stable *bag3*$^{e2/e2}$;*myh9b*$^{e12/+}$ double mutant. Together, these data indicated that effective gene knockdown in adult F0 animals can be incurred by injection of a predicted MMEJ-inducing sgRNA, enabling reliable establishment of genotype-phenotype relationship. The success of this genetic technology platform effectively minimalizes the need of multi-generation genetic crossing to assess genetic modifying effects, representing a rapid approach for discovering modifier genes for an adult-onset disease such as cardiomyopathy.

The use of MENTHU, a double-strand break repair prediction algorithm, helped identify sgRNAs with a predictable genetic lesion with high knockdown efficiency. Based on TIDE analysis, sgRNAs for 8 DE genes induced a predicted microhomology allele in the targeted loci at rates ranging from 49.8% to 93.9% among all 8 genetic lesions in F0 adult fish (Table 1). 7 out of 8 targeted loci incurred >50% KO score upon the first try. Of note, we used a single predicted MMEJ-inducing sgRNA for each gene, which differs from recent F0-based embryonic studies using NHEJ-inducing sgRNAs, whereby 3-4 sgRNAs against the same target gene were co-injected (Hoshijima et al., 2019; Kroll et al., 2021; Wu et al., 2018). This is likely because high knockout (KO) efficiency is needed in embryonic studies to generate biallelic alleles that recapitulate stable homozygous mutants. Co-injection of multiple sgRNAs effectively overcomes the confounding factor that about 1/3 of indels induced by each sgRNA do not shift the reading frame. By contrast, assessment of modifier effects in adult zebrafish does not require extremely high KO score, whereby ~50% KO score would be sufficient. Importantly, the ratio of non-reading frame shifting indels would be much lower in fish injected with predicted MMEJ-inducing sgRNAs than with NHEJ-inducing sgRNAs.

Disease Models & Mechanisms • DMM • Accepted manuscript

We acknowledge several shortcomings of this F0-based genetic assay, most of which are associated with the complicated genetic nature. First, unlike a stable mutant that harbors a single genetic lesion, each F0 fish harbors a mixture of different genetic lesions in the same genomic locus, including those that do not shift the reading frame. Because of this concern, we favor the predicted MMEJ-inducing sgRNAs over the normal CRISPR sgRNAs, since majority of the genetic lesions are the predicted deletion alleles that shift the reading frame. Second, phenotypes in stable double mutants might not be fully recapitulated in F0 mutants. For example, the *bag3*$^{e2/e2}$;*dnajb6b*$^{e6\text{-}MJ}$ double mutants manifested milder phenotypes than either *bag3*$^{e2/e2}$;*dnajb6b*$^{-/-}$ or *bag3*$^{e2/e2}$; *dnajb6b*$^{+/-}$ double mutant, both of which died within 5 weeks. While *bag3*$^{e2/e2}$;*dnajb6b*$^{e6\text{-}MJ}$ did recapitulate several adult cardiac phenotypes in the *bag3*$^{e2/+}$;*dnajb6b*$^{-/-}$ double mutant fish (Fig. 4), it didn't recapitulate the jaw protruding phenotype. We postulated that one potential reason is that a 50% KO score in F0 fish does not equal to a stable heterozygous mutant, whereby all cells contain a genetic lesion in one of the two alleles. Instead, cells in the F0 fish might be a mixture that consists of cells with no genetic lesion, with a single genetic lesion, and with biallelic genetic lesions. Another potential reason is the different functional consequence between the F0*dnajb6b*$^{e6\text{-}MJ}$ and stable *dnajb6b*$^{+/-}$ on *bag3* cardiomyopathy. While the predicted genetic lesions incurred by the predicted MMEJ-inducing sgRNA presumably lead to truncated peptides and is of loss-of-function nature, more experimental evidence is needed. Third, because phenotypic assays were performed in the F0 generation, off-target effects of the sgRNA might exist and confound phenotyping interpretation. However, despite these shortcomings, genotype-phenotype relationships can still be largely established in adult fish, as indicated by the three experimental evidences summarized earlier in the discussion. To ultimately address these limitations, we strongly recommend to confirm candidate genetic interactions by generating stable double mutants, which is readily available at F1.

Disease Models & Mechanisms • DMM • Accepted manuscript

The discovery of novel genetic modifiers suggested pathophysiology of an inherited cardiomyopathy

In this manuscript, we initially identified the modifying effects of *dnajb6b* genetic deficiency on *bag3* cardiomyopathy through a classic genetic analysis. Together with *mtor* as another common genetic modifier between *bag3* cardiomyopathy and AIC, this data endorsed the concept that cardiomyopathies of different etiology share common pathological pathways (Tadros et al., 2021). Thus, one plausible future strategy for discovering genetic modifiers of an inherited cardiomyopathy would be to test candidate genetic modifiers of AIC that will be obtained by larger scale forward genetic screens in zebrafish.

Identification of new modifier genes for a human disease are helpful to unveil new pathophysiologic mechanisms, aiding the development of disease intervention. For example, the discovery of disruption of *dnajb6b* gene function as a deleterious modifier for anthracycline-induced cardiomyopathy (AIC) suggested unfolded protein response (UPR) as the downstream signaling, and overexpression of *dnajb6b* gene in cardiomyocytes as a therapeutic avenue (Ding et al., 2016); the discovery of *rxraa* as a salutary modifier for AIC suggested defective endothelial barrier function as a pathological event in the early phase of AIC, and activation of retinoic acid (RA) signaling as a therapeutic avenue (Ding et al., 2016; Ma et al., 2020). Here, we unveiled the modifying effects of *dnajb6b* genetic deficiency on *bag3* cardiomyopathy. Because *dnajb6b* encodes a co-chaperone protein that facilitates the degradation of misfolded proteins, and that increased protein aggregation was detected in the *bag3;dnajb6b* co-deficient fish, we speculate that Dnajb6b works synergistically with the Bag3 protein to regulate proteostasis. Moreover, our F0-based genetic screen also identified *myh9b* as a new modifying gene, which was later confirmed by stable double mutants. *myh9b* encodes a cytoskeletal protein that plays an important role in the initiation step of autophagy (Kruppa et al., 2016). Specifically, Myh9b functions downstream of Ulk1 and Atg8, regulating phagophore formation.

Disease Models & Mechanisms • DMM • Accepted manuscript

Cosistent with this notion, we observed further decreased LC3 II level in the *bag3;myh9b* double mutant (Fig. 7E). Intriguingly, our previous data identified mTOR as a salutary modifier, which functions upstream of Ulk1 to govern the initiation of autophagy (Suvorova and Pospelov, 2019). These data suggest that *bag3* mediated cardiomyopathy is characterized with high sensitivity to genetic lesions in the *mtor-myh9b* signaling axis that affects autophagy initiation, a key step of proteostasis. Further studies are warranted to elucidate detailed mechanisms underlying the modifying effects of *myh9b* on *bag3* cardiomyopathy.

In summary, we proved the feasibility of a F0-based genetic assay in adult fish, which possesses much higher throughput than classic genetic interaction studies using stable double mutants. As suggested by our pilot screen, the assay is particularly useful in experimentally testing vast number of candidate genes suggested from system biology approaches such as DE genes identified from transcriptome analysis. Thus, it is anticipated that our assay would facilitate systematic discovery of genetic modifiers for inherited cardiomyopathies. In principle, this F0 based genetic assay should be applicable to other human diseases that can be modeled in the zebrafish.

MATERIAL AND METHODS

Animals

Zebrafish(Danio rerio) WIK were maintained under a 14 hours light–10 hours dark cycle at 28.5°C and handled with care. The animal study protocols were approved by the Mayo Clinic Institutional Animal Care and Use Committee (A3513). All animal study procedures were performed in accordance with the Guide for the Care and Use of Laboratory Animals published by the US National Institutes of Health (NIH Publication No. 85-23, revised 1996). The *bag3*$^{e2/e2}$ mutants containing 10-nucleotides deletion in the 2nd exon were reported previously (Ding et al.,

Disease Models & Mechanisms • DMM • Accepted manuscript

2019). Genotyping to discern the *bag3* mutant from WT siblings was carried out by PCR followed by digestion with the restriction enzyme Pst I. The gene-break transposon (*GBT) 002/sorbs2b, GBT136/ano5a, GBT411/dnajb6b*, and *GBT419/rxraa* mutants were generated and reported previously (Ding et al., 2013; Ding et al., 2016), and the mutant alleles were identified by genotyping PCR using gene-specific primer pairs flanking the GBT transposon integration site combined with a RP2 insertional vector-specific primer RP2-5'-LTR or RP2-3'-LTR (Ding et al., 2013). Primer sequences for genotyping PCR are listed in Supplemental Table 1.

In vivo echocardiography for adult fish hearts

The Vevo 3100 high-frequency imaging system equipped with a 50 MHz (MX700) linear array transducer (FUJIFILM VisualSonics Inc) was used to measure cardiac function indices in adult zebrafish according to reported protocol (Zhang et al., 2018). Briefly, acoustic gel (Aquasonic® 100, Parker Laboratories, Inc) was applied over the surface of the transducer to provide adequate coupling with the tissue interface. Adult zebrafish at appropriate ages were anesthetized in tricaine (0.02%) for 5 minutes, placed ventral side up into a sponge. The MX700 transducer was placed above the zebrafish to provide a sagittal imaging plane for the heart. B-mode images were acquired with an imaging field of view of 9.00 mm in the axial direction and 5.73 mm in the lateral direction, a frame rate of 123 Hz, with medium persistence and a transmit focus at the center of the heart. Image quantification was performed using the VevoLAB workstation. Cardiac function indices of the ejection fraction (EF) was calculated using the formula: EF=(EDV−ESV)/EDV, and fractional shortening (FS) was calculated using the formula: FS=(Ld−Ls)/Ld. EDV and ESV are the ventricular volumes at the end-diastolic stage and end-systolic stage, respectively. Ventricular chamber dimensions were measured from B-mode images using the following two indices: EDV/body weight (BW) and ESV/BW (Zhang et al., 2018). Ld and Ls represent the length of the short axis of the ventricle at the end-diastolic stage

Disease Models & Mechanisms • DMM • Accepted manuscript

and end-systolic stage, respectively. For each index on individual fish, measurements were performed on 3 independent cardiac cycles to acquire average values.

Embryonic heart function evaluation

The quantification of zebrafish embryonic heart function was performed using previously reported protocols.(Hoage et al., 2012) Briefly, fish embryos at designated stages were anesthetized with tricaine (0.02%) (Argent Chemical Laboratories) for 2 min, placed lateral side up, and held in place with 3% methyl cellulose (Sigma-Aldrich). The beating hearts were documented using a Zeiss Axioplan 2 microscope with the differential interference camera lens and fraction shortening (FS) were analyzed by Image J and calculated using the formula [FS=(Ld−Ls)/Ld]. Ld and Ls represent the length of the short axis of the ventricle at the end-diastolic stage and end-systolic stage, respectively.

Measurement of the ventricular surface area to body weight ratio

The measurement of ventricular surface area (VSA) to body weight (BW) ratio was performed according to a previously published method (Ding et al., 2011). To measure body weight, fish were anesthetized in 0.16-mg/mL tricaine solution, semi-dried on a paper towel, and weighted on a scale. To measure the VSA, ventricles of individual zebrafish were dissected and imaged next to a millimeter ruler under a Leica MZ FLI III microscope. The largest projection of a ventricle was outlined using ImageJ software. The VSA/BW index was then calculated by the largest projection area of ventricle (in mm^2) divided by body weight (in gram).

Histology and transmission electron microscopy

For the hematoxylin and eosin (H&E) staining, heart tissues were dissected from individual adult fish at the designed stages after euthanasia by incubation with 0.032% tricaine for 10 minutes. Isolated hearts were immediately fixed in 4% PBS-buffered formaldehyde and sent to the Mayo

Disease Models & Mechanisms • DMM • Accepted manuscript

Clinic Histology Core Laboratory for subsequent sample processing and hematoxylin and eosin (H&E) staining. Images of the apex region were captured using the EVOS FL Auto Imaging System (ThermoFisher Scientific). The density of the trabecular muscle was quantified using ImageJ software. For the transmission electron microscopy (TEM) study, adult zebrafish hearts at designated stages were dissected and immediately fixed in the fixation solution (4% paraformaldehyde and 1% glutaraldehyde in 0.1 M phosphate buffer [pH, 7.2]) at room temperature for 1 hour, followed by overnight incubation at 4°C. Fixed samples were subsequently processed and imaged at the Mayo Clinic Electron Microscopy Core Facility using a Philips CM10 transmission electron microscope.

Western blotting

Either individual fish embryos at 1-3 days post-fertilization (for Fig. 3C) or individually isolated adult fish heart ventricle (for Fig. 2E, 3E and 4G) were transferred to the RIPA lysis buffer (Sigma-Aldrich) supplemented with complete protease inhibitor cocktail (Roche) and homogenized using a Bullet Blender tissue homogenizer (Next Advance, Inc). About 1-5 μg resultant protein lysates were subject to western blotting using a standard protocol. The following primary antibodies were used: anti-Gapdh (1:5,000, Santa Cruz Biotechnology Inc., catalog # sc-25778), anti-mTOR (1:3,000, Cell Signaling Technology, catalog # 2983), anti-ubiquitin (1:1,000, ThermoFisher Scientific, catalog # PA5-17067), and anti-LC3 (1:3,000, Cell Signaling Technology, catalog #12741). All these antibodies were demonstrated to work in zebrafish as reported previously (Bu et al., 2021; Ding et al., 2019).

Predicted MMEJ-based single guide RNA design and F0 injection

Sequences for genes of interest were acquired and downloaded from the Ensemble (http://useast.ensembl.org/index.html). Preferred exons located toward the N-terminal were then uploaded to an online algorithm, MENTHU (http://genesculpt.org/menthu/) for guide RNA target

Disease Models & Mechanisms • DMM • Accepted manuscript

selection. Target sequences with scores > 1.0 were chosen from predicted MMEJ loci (Table 1). Single guide RNAs (sgRNAs) with appropriate chemical modifications were synthesized and obtained from the Synthego (Synthego Corporation). sgRNAs were dissolved in nuclease-free duplex buffer (Integrated DNA Technologies, 11-01-03-01) to obtain 100 µM concentration as stock solutions and were further diluted to 2 µM to 10 µM as working concentrations.

The Alt-R Cas9 protein (Integrated DNA Technologies, 1081058) was diluted to the working concentration of 3.3 µg/µL in buffer (20 mM HEPES, 100 mM NaCl, 5 mM $MgCl_2$, 0.1 mM EDTA at pH 7.5). The sgRNA and Cas9 protein diluted to working concentrations were then mixed at a ratio of 1:1 volume (1.5 µl of gRNA+1.5 µl of Cas9 protein) and incubated in a 37°C water bath for 10 min to assemble the sgRNA-Cas9 protein (sgRNP) complex. ~1 nL of the sgRNP complex with 0.01% phenol red indicator was then injected to one-cell stage fish embryos to obtain the predicted MMEJ injected F0 embryos. For each predicted MMEJ-inducing sgRNA, we tested different injection doses and usually measured KO score in 8 injected embryos, aiming to identify sgRNAs that could result in >50% KO score in all injected embryos. After the injected embryos reached adult stage, we confirm the efficiency of sgRNAs by measuring KO score again via performing genotyping PCR using genomic DNA isolated from tail fin. We carried out phenotyping analysis on all animals injected with the same sgRNA, and deprioritized sgRNAs with lower KO scores.

Knockout (KO) score calculation

Either individual predicted MMEJ sgRNPs injected embryos or tail fin from adult fish were collected and transferred to 50 µL alkaline lysis buffer (25 mM NaOH, 0.2 mM EDTA, pH 12) and incubated for 30 minutes at 95°C, followed by adding 50 µL neutralization buffer (40 mM Tris-HCl, pH 5.0). 1 µL of resultant genomic DNA lysates were used as templates for PCR analysis to quantify KO score for each predicted MMEJ sgRNA. The PCR primer sequence

Disease Models & Mechanisms • DMM • Accepted manuscript

information for KO score quantification is listed in Supplemental Table 3. To quantify the score, 5 µL PCR amplicon was digested with Exo I and subsequently sent for Sanger sequencing at Genewiz (https://clims4.genewiz.com/CustomerHome/Index). The chromatograms from two PCR amplicons using either predicted MMEJ sgRNA injected or uninjected embryonic genomic DNA lysates as templates were analyzed for KO score calculation using the R code-based open access software Inference of CRISPR Edits (ICE) v2 CRISPR Analysis Tool by TIDE (https://www.synthego.com/products/bioinformatics/crispr-analysis) (Brinkman and van Steensel, 2019). Percent microhomology allele was calculated by dividing the KO score for the predicted microhomology indel by the total KO score.

Quantitative reverse transcription (RT) PCR

Total RNA was extracted from a single zebrafish larvae or an individual adult fish ventricle using Trizol reagent (ThermoFisher Scientific) following the manufacturer's instruction. Approximately 100 ng total RNA was used for reverse transcription (RT) and cDNA synthesis using Superscript III First-Strand Synthesis System (ThermoFisher Scientific). Real-time quantitative RT-PCR was run in 96-well optical plates (ThermoFisher Scientific) using an Applied Biosystem VAii 7 System (ThermoFisher Scientific). Gene expression levels were normalized using the expression level of either glyceraldehyde 3-phosphate dehydrogenase (*gapdh) or actin, beta 2 (actb2)* by –ΔΔCt (cycle threshold) values. All quantitative RT-PCR primer sequences were listed in Supplemental Table 2.

Co-immunoprecipitation assay

Human DNAJB6 cDNA was synthesized from total RNA isolated from normal human adult heart (Biochain) by RT-PCR and cloned into a pShuttle plasmid in frame with the Flag tag (Addgene), resulting in the generation of pShuttle-DNAJB6-Flag construct. Human BAG3 cDNA was synthesized from total RNA isolated from normal human adult heart and was cloned into the

Disease Models & Mechanisms • DMM • Accepted manuscript

pShuttle plasmid in frame with the HA tag (Addgene), resulted in the generation of pShuttle-BAG3-HA construct. 1 µg of either single or double constructs were transfected into HEK293 cell (about 80% confluency) in a p10 dish. Co-immunoprecipitation experiments were carried out using the FLAG® Immunoprecipitation Kit (FLAGIPT1, Sigma) according to the manufacture's instruction. Anti-Flag antibody (1:10,000 Sigma) and anti-HA antibody (1:10,000 Sigma) were used.

Statistics

No sample sizes were calculated before performing the experiments. No animals were excluded for analysis. The unpaired two-tailed Student's *t*-test was used to compare 2 groups. One-way analysis of variance (ANOVA) was used to assess differences among 3 or more groups. For the animal survival rate comparison, the log-rank test was used to determine the difference. Survival curves were cumulative results using fish obtained from several breeding efforts. For all dot plots, each value represents mean ± standard error (SE). Sample size (N) indicates number of animals. All statistical analyses were performed with the GraphPad Prism 7. For the post hoc analysis, Tukey's test was employed to confirm the findings.

Acknowledgments

We thank Beninio T. Gore and Kashia B. Stragey for maintaining our zebrafish facility. We also thank Matthew H. Koslow for editing the manuscript.

Competing interests

The authors declare no competing or financial interests.

Disease Models & Mechanisms • DMM • Accepted manuscript

Author contributions

Conceptualization: Y.D., M.W. and X.X.; Methodology: Y.D., M.W., H.B., J.L. and X.X.; Software: Y.D. and M.W.; Validation: Y.D. M.W. and X.X.; Formal analysis: Y.D., M.W. and X.X; Investigation: Y.D., M.W. and X.X.; Data curation: Y.D., M.W., H.B. and J.L.; Writing - original draft: Y.D., M.W. and X.X.; Writing - review & editing: Y.D., X.L., and X.X.; Supervision: Y.D., X.L., and X.X.; Project administration: Y.D., M.W. and X.X.; and Funding acquisition: X.X. H.B. and M.W.

Funding

This work was supported in part by grants from NIH (HL107304, HL081753) and the Mayo Foundation to X.X. Mingming Wang and Haisong Bu are funded by the China Scholarship Council (201706557083 to M.W., CSC201906370239 to H.B.).

References

Arad, M., Seidman, J. G. and Seidman, C. E. (2002). Phenotypic diversity in hypertrophic cardiomyopathy. *Hum Mol Genet* **11**, 2499-506.

Ata, H., Ekstrom, T. L., Martinez-Galvez, G., Mann, C. M., Dvornikov, A. V., Schaefbauer, K. J., Ma, A. C., Dobbs, D., Clark, K. J. and Ekker, S. C. (2018). Robust activation of microhomology-mediated end joining for precision gene editing applications. *PLoS Genet* **14**, e1007652.

Brinkman, E. K. and van Steensel, B. (2019). Rapid Quantitative Evaluation of CRISPR Genome Editing by TIDE and TIDER. *Methods Mol Biol* **1961**, 29-44.

Bu, H., Ding, Y., Li, J., Zhu, P., Shih, Y. H., Wang, M., Zhang, Y., Lin, X. and Xu, X. (2021). Inhibition of mTOR or MAPK ameliorates vmhcl/myh7 cardiomyopathy in zebrafish. *JCI Insight* **6**.

Daw, E. W., Lu, Y., Marian, A. J. and Shete, S. (2008). Identifying modifier loci in existing genome scan data. *Annals of human genetics* **72**, 670-5.

Deacon, D. C., Happe, C. L., Chen, C., Tedeschi, N., Manso, A. M., Li, T., Dalton, N. D., Peng, Q., Farah, E. N., Gu, Y. et al. (2019). Combinatorial interactions of genetic variants in human cardiomyopathy. *Nat Biomed Eng* **3**, 147-157.

Ding, Y., Dvornikov, A. V., Ma, X., Zhang, H., Wang, Y., Lowerison, M., Packard, R. R., Wang, L., Chen, J., Zhang, Y. et al. (2019). Haploinsufficiency of mechanistic target of rapamycin ameliorates bag3 cardiomyopathy in adult zebrafish. *Dis Model Mech* **12**.

Ding, Y., Liu, W., Deng, Y., Jomok, B., Yang, J., Huang, W., Clark, K. J., Zhong, T. P., Lin, X., Ekker, S. C. et al. (2013). Trapping cardiac recessive mutants via expression-based insertional mutagenesis screening. *Circ Res* **112**, 606-17.

Disease Models & Mechanisms • DMM • Accepted manuscript

Ding, Y., Long, P. A., Bos, J. M., Shih, Y. H., Ma, X., Sundsbak, R. S., Chen, J., Jiang, Y., Zhao, L., Hu, X. et al. (2016). A modifier screen identifies DNAJB6 as a cardiomyopathy susceptibility gene. *JCI Insight* **1**.

Ding, Y., Sun, X., Huang, W., Hoage, T., Redfield, M., Kushwaha, S., Sivasubbu, S., Lin, X., Ekker, S. and Xu, X. (2011). Haploinsufficiency of target of rapamycin attenuates cardiomyopathies in adult zebrafish. *Circ Res* **109**, 658-69.

Ding, Y., Yang, J., Chen, P., Lu, T., Jiao, K., Tester, D. J., Giudicessi, J. R., Jiang, K., Ackerman, M. J., Li, Y. et al. (2020). Knockout of SORBS2 Protein Disrupts the Structural Integrity of Intercalated Disc and Manifests Features of Arrhythmogenic Cardiomyopathy. *J Am Heart Assoc* **9**, e017055.

Dominguez, F., Cuenca, S., Bilinska, Z., Toro, R., Villard, E., Barriales-Villa, R., Ochoa, J. P., Asselbergs, F., Sammani, A., Franaszczyk, M. et al. (2018). Dilated Cardiomyopathy Due to BLC2-Associated Athanogene 3 (BAG3) Mutations. *J Am Coll Cardiol* **72**, 2471-2481.

Dorn, G. W., 2nd. (2011). The genomic architecture of sporadic heart failure. *Circulation Research* **108**, 1270-83.

Fang, X., Bogomolovas, J., Wu, T., Zhang, W., Liu, C., Veevers, J., Stroud, M. J., Zhang, Z., Ma, X., Mu, Y. et al. (2017). Loss-of-function mutations in co-chaperone BAG3 destabilize small HSPs and cause cardiomyopathy. *J Clin Invest* **127**, 3189-3200.

Gifford, C. A., Ranade, S. S., Samarakoon, R., Salunga, H. T., de Soysa, T. Y., Huang, Y., Zhou, P., Elfenbein, A., Wyman, S. K., Bui, Y. K. et al. (2019). Oligogenic inheritance of a human heart disease involving a genetic modifier. *Science* **364**, 865-870.

Goldberg, I. J., Reue, K., Abumrad, N. A., Bickel, P. E., Cohen, S., Fisher, E. A., Galis, Z. S., Granneman, J. G., Lewandowski, E. D., Murphy, R. et al. (2018). Deciphering the Role of Lipid Droplets in Cardiovascular Disease: A Report From the 2017 National Heart, Lung, and Blood Institute Workshop. *Circulation* **138**, 305-315.

Henning, R. H. and Brundel, B. (2017). Proteostasis in cardiac health and disease. *Nat Rev Cardiol* **14**, 637-653.

Hershberger, R. E., Hedges, D. J. and Morales, A. (2013). Dilated cardiomyopathy: the complexity of a diverse genetic architecture. *Nature reviews. Cardiology* **10**, 531-47.

Hoage, T., Ding, Y. and Xu, X. (2012). Quantifying cardiac functions in embryonic and adult zebrafish. *Methods Mol Biol* **843**, 11-20.

Hoshijima, K., Jurynec, M. J., Klatt Shaw, D., Jacobi, A. M., Behlke, M. A. and Grunwald, D. J. (2019). Highly Efficient CRISPR-Cas9-Based Methods for Generating Deletion Mutations and F0 Embryos that Lack Gene Function in Zebrafish. *Dev Cell* **51**, 645-657 e4.

Hwang, J. W., Jang, M. A., Jang, S. Y., Seo, S. H., Seong, M. W., Park, S. S., Ki, C. S. and Kim, D. K. (2017). Diverse Phenotypic Expression of Cardiomyopathies in a Family with TNNI3 p.Arg145Trp Mutation. *Korean Circ J* **47**, 270-277.

Kroll, F., Powell, G. T., Ghosh, M., Gestri, G., Antinucci, P., Hearn, T. J., Tunbak, H., Lim, S., Dennis, H. W., Fernandez, J. M. et al. (2021). A simple and effective F0 knockout method for rapid screening of behaviour and other complex phenotypes. *Elife* **10**.

Kruppa, A. J., Kendrick-Jones, J. and Buss, F. (2016). Myosins, Actin and Autophagy. *Traffic* **17**, 878-90.

Le Corvoisier, P., Park, H. Y., Carlson, K. M., Marchuk, D. A. and Rockman, H. A. (2003). Multiple quantitative trait loci modify the heart failure phenotype in murine cardiomyopathy. *Hum Mol Genet* **12**, 3097-107.

Ma, X., Zhu, P., Ding, Y., Zhang, H., Qiu, Q., Dvornikov, A. V., Wang, Z., Kim, M., Wang, Y., Lowerison, M. et al. (2020). Retinoid X receptor alpha is a spatiotemporally predominant therapeutic target for anthracycline-induced cardiotoxicity. *Sci Adv* **6**, eaay2939.

Disease Models & Mechanisms • DMM • Accepted manuscript

Martinez-Galvez, G., Joshi, P., Friedberg, I., Manduca, A. and Ekker, S. C. (2021). Deploying MMEJ using MENdel in precision gene editing applications for gene therapy and functional genomics. *Nucleic Acids Res* **49**, 67-78.

Mouton, J. M., van der Merwe, L., Goosen, A., Revera, M., Brink, P. A., Moolman-Smook, J. C. and Kinnear, C. (2016). MYBPH acts as modifier of cardiac hypertrophy in hypertrophic cardiomyopathy (HCM) patients. *Hum Genet* **135**, 477-483.

Myers, V. D., McClung, J. M., Wang, J., Tahrir, F. G., Gupta, M. K., Gordon, J., Kontos, C. H., Khalili, K., Cheung, J. Y. and Feldman, A. M. (2018). The Multifunctional Protein BAG3: A Novel Therapeutic Target in Cardiovascular Disease. *JACC Basic Transl Sci* **3**, 122-131.

Norton, N., Li, D., Rieder, M. J., Siegfried, J. D., Rampersaud, E., Zuchner, S., Mangos, S., Gonzalez-Quintana, J., Wang, L., McGee, S. et al. (2011). Genome-wide studies of copy number variation and exome sequencing identify rare variants in BAG3 as a cause of dilated cardiomyopathy. *Am J Hum Genet* **88**, 273-82.

Pantou, M. P., Gourzi, P., Gkouziouta, A., Tsiapras, D., Zygouri, C., Constantoulakis, P., Adamopoulos, S. and Degiannis, D. (2018). Phenotypic Heterogeneity within Members of a Family Carrying the Same RBM20 Mutation R634W. *Cardiology* **141**, 150-155.

Ruparelia, A. A., McKaige, E. A., Williams, C., Schulze, K. E., Fuchs, M., Oorschot, V., Lacene, E., Meregalli, M., Lee, C., Serrano, R. J. et al. (2020). Metformin rescues muscle function in BAG3 myofibrillar myopathy models. *Autophagy*, 1-17.

Sarparanta, J., Jonson, P. H., Golzio, C., Sandell, S., Luque, H., Screen, M., McDonald, K., Stajich, J. M., Mahjneh, I., Vihola, A. et al. (2012). Mutations affecting the cytoplasmic functions of the co-chaperone DNAJB6 cause limb-girdle muscular dystrophy. *Nat Genet* **44**, 450-5, S1-2.

Sen-Chowdhry, S., Syrris, P., Pantazis, A., Quarta, G., McKenna, W. J. and Chambers, J. C. (2010). Mutational heterogeneity, modifier genes, and environmental influences contribute to phenotypic diversity of arrhythmogenic cardiomyopathy. *Circulation. Cardiovascular genetics* **3**, 323-30.

Shen, M. W., Arbab, M., Hsu, J. Y., Worstell, D., Culbertson, S. J., Krabbe, O., Cassa, C. A., Liu, D. R., Gifford, D. K. and Sherwood, R. I. (2018). Predictable and precise template-free CRISPR editing of pathogenic variants. *Nature* **563**, 646-651.

Su, M., Wang, J., Kang, L., Wang, Y., Zou, Y., Feng, X., Wang, D., Ahmad, F., Zhou, X., Hui, R. et al. (2014). Rare variants in genes encoding MuRF1 and MuRF2 are modifiers of hypertrophic cardiomyopathy. *Int J Mol Sci* **15**, 9302-13.

Suvorova, II and Pospelov, V. A. (2019). AMPK/Ulk1-dependent autophagy as a key mTOR regulator in the context of cell pluripotency. *Cell Death Dis* **10**, 260.

Suzuki, M., Carlson, K. M., Marchuk, D. A. and Rockman, H. A. (2002). Genetic modifier loci affecting survival and cardiac function in murine dilated cardiomyopathy. *Circulation* **105**, 1824-9.

Tadros, R., Francis, C., Xu, X., Vermeer, A. M. C., Harper, A. R., Huurman, R., Kelu Bisabu, K., Walsh, R., Hoorntje, E. T., Te Rijdt, W. P. et al. (2021). Shared genetic pathways contribute to risk of hypertrophic and dilated cardiomyopathies with opposite directions of effect. *Nat Genet* **53**, 128-134.

Visscher, P. M., Brown, M. A., McCarthy, M. I. and Yang, J. (2012). Five years of GWAS discovery. *American journal of human genetics* **90**, 7-24.

Wende, A. R. and Abel, E. D. (2010). Lipotoxicity in the heart. *Biochim Biophys Acta* **1801**, 311-9.

Wheeler, F. C., Fernandez, L., Carlson, K. M., Wolf, M. J., Rockman, H. A. and Marchuk, D. A. (2005). QTL mapping in a mouse model of cardiomyopathy reveals an ancestral modifier allele affecting heart function and survival. *Mamm Genome* **16**, 414-23.

Disease Models & Mechanisms • DMM • Accepted manuscript

Wheeler, F. C., Tang, H., Marks, O. A., Hadnott, T. N., Chu, P. L., Mao, L., Rockman, H. A. and Marchuk, D. A. (2009). Tnni3k modifies disease progression in murine models of cardiomyopathy. *PLoS Genet* **5**, e1000647.

Wu, R. S., Lam, II, Clay, H., Duong, D. N., Deo, R. C. and Coughlin, S. R. (2018). A Rapid Method for Directed Gene Knockout for Screening in G0 Zebrafish. *Dev Cell* **46**, 112-125 e4.

Zhang, H., Dvornikov, A. V., Huttner, I. G., Ma, X., Santiago, C. F., Fatkin, D. and Xu, X. (2018). A Langendorff-like system to quantify cardiac pump function in adult zebrafish. *Dis Model Mech* **11**.

Disease Models & Mechanisms • DMM • Accepted manuscript

Figures

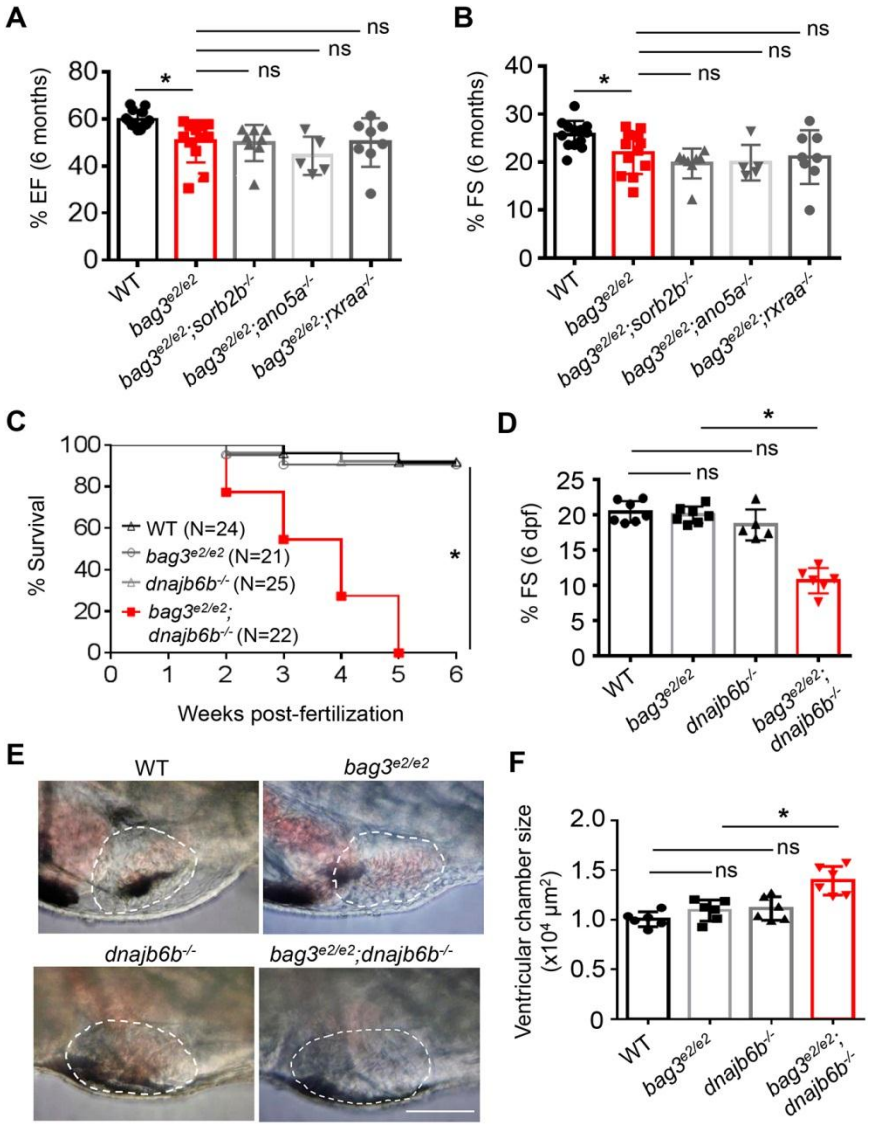

Fig. 1. **A genetic testing identified *GBT411/dnajb6* as a deleterious modifier for *bag3* cardiomyopathy**

A-B. Percent ejection fraction (EF) (A) and fractional shortening (FS) (B) of *bag3*$^{e2/e2}$ *;sorbs2b*$^{-/-}$, *bag3*$^{e2/e2}$*;ano5a*$^{-/-}$ and *bag3*$^{e2/e2}$*;rxraa*$^{-/-}$ double mutant fish compared to *bag3*$^{e2/e2}$ single mutants and WT controls at 6 months. N=6-15, one-way ANOVA. **C,** Survival curves of *bag3*$^{e2/e2}$*;GB411*$^{-}$

Disease Models & Mechanisms • DMM • Accepted manuscript

$^{-/-}$ double mutant fish compared to single mutants and WT controls. N=15-24, log rank test. **D**, FS of *bag3*$^{e2/e2}$*;dnajb6b*$^{-/-}$ double mutants compared to single mutants and WT controls at 6 days post-fertilization (dpf). N=6-7, one-way ANOVA. **E-F,** Ventricular chamber outlines (E) and size quantification of *bag3*$^{e2/e2}$*;GB411*$^{-/-}$ double mutant hearts at systolic stage compared to single mutants and WT controls. N=6. One-way ANOVA. Scale bar, 100 µm. *, *P*<0.05. ns, not significant.

Disease Models & Mechanisms • DMM • Accepted manuscript

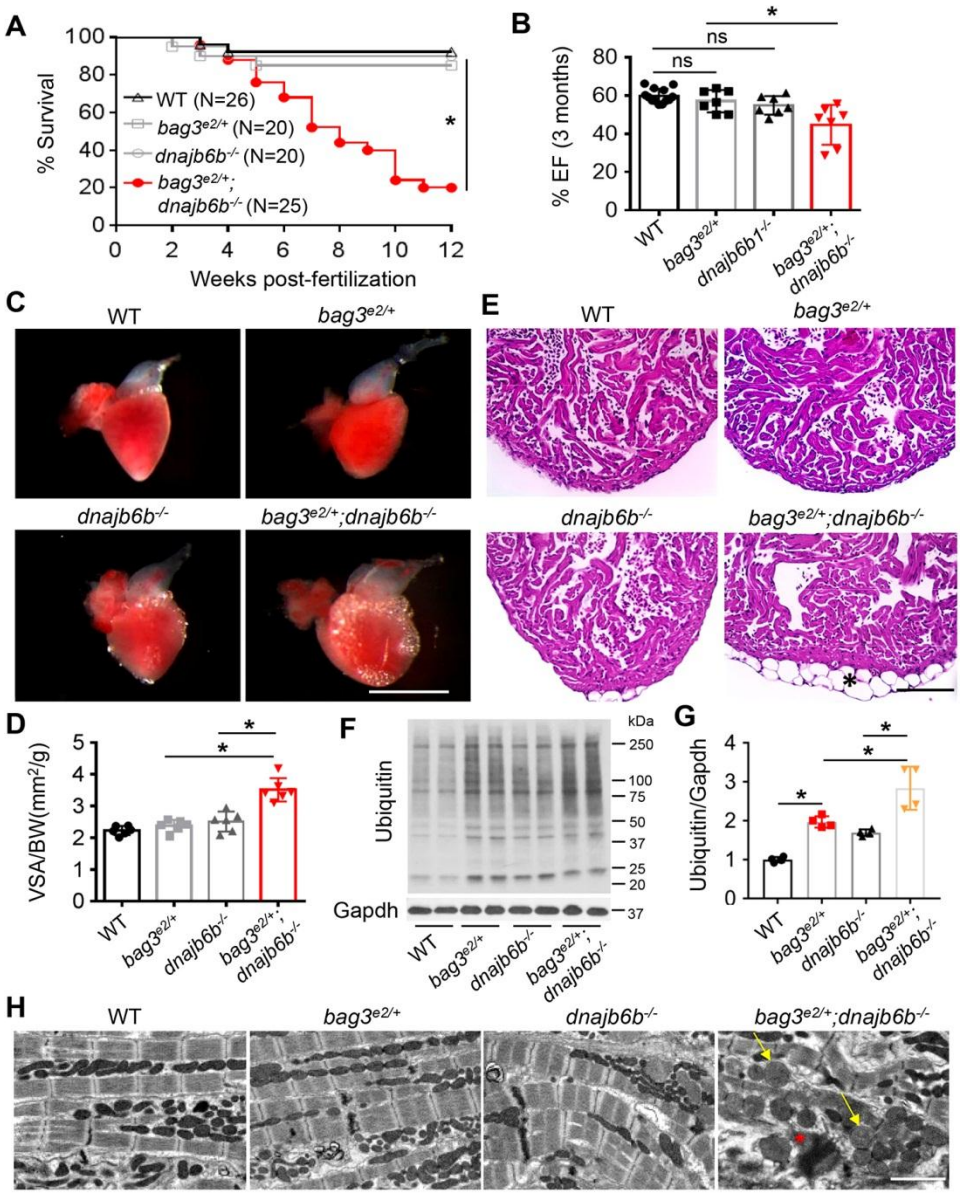

Fig. 2. Genetic interaction between *bag3*$^{e2/+}$ and *dnajb6b*$^{-/-}$ in an adult heart

A, Survival curves of *bag3*$^{e/+}$*;GB411*$^{-/-}$ double mutant fish compared to single mutants and WT controls. N=25-40, log rank test**. B**, EF of *bag3*$^{e2/+}$*;dnajb6b*$^{-/-}$ double mutants compared to single mutants and WT controls at 3 months post-fertilization. N=6-8, one-way ANOVA. **C-E,** The *bag3*$^{e2/+}$*;dnajb6b*$^{-/-}$ double mutant fish manifested significantly enlarged ventricular surface area (VSA) normalized by body weight (BW) index (C-D) and obvious lipid accumulation phenotypes (indicated by the star) (E). N=3-4, one-way ANOVA. Scale bar in C, 1 mm. Scale *bar in D, 100*

Disease Models & Mechanisms • DMM • Accepted manuscript

μM. ***F-G,*** *Western blot and quantification analysis of ubiquitinated protein levels* in heart lysates of *bag3*$^{e2/+}$*;dnajb6b*$^{-/-}$ double mutant fish compared to single mutants and WT controls at 3 months. N=4, one-way ANOVA. **H,** Confirmative images of transmission electron microscope (TEM) showed that mitochondrial swelling (arrows) and myofibril degeneration phenotypes (star) detected in the *bag3*$^{e2/+}$*;dnajb6b*$^{-/-}$ double mutant fish hearts at 3 months. Scale bar, 2 μM. *, *P*<0.05. ns, not significant.

Disease Models & Mechanisms • DMM • Accepted manuscript

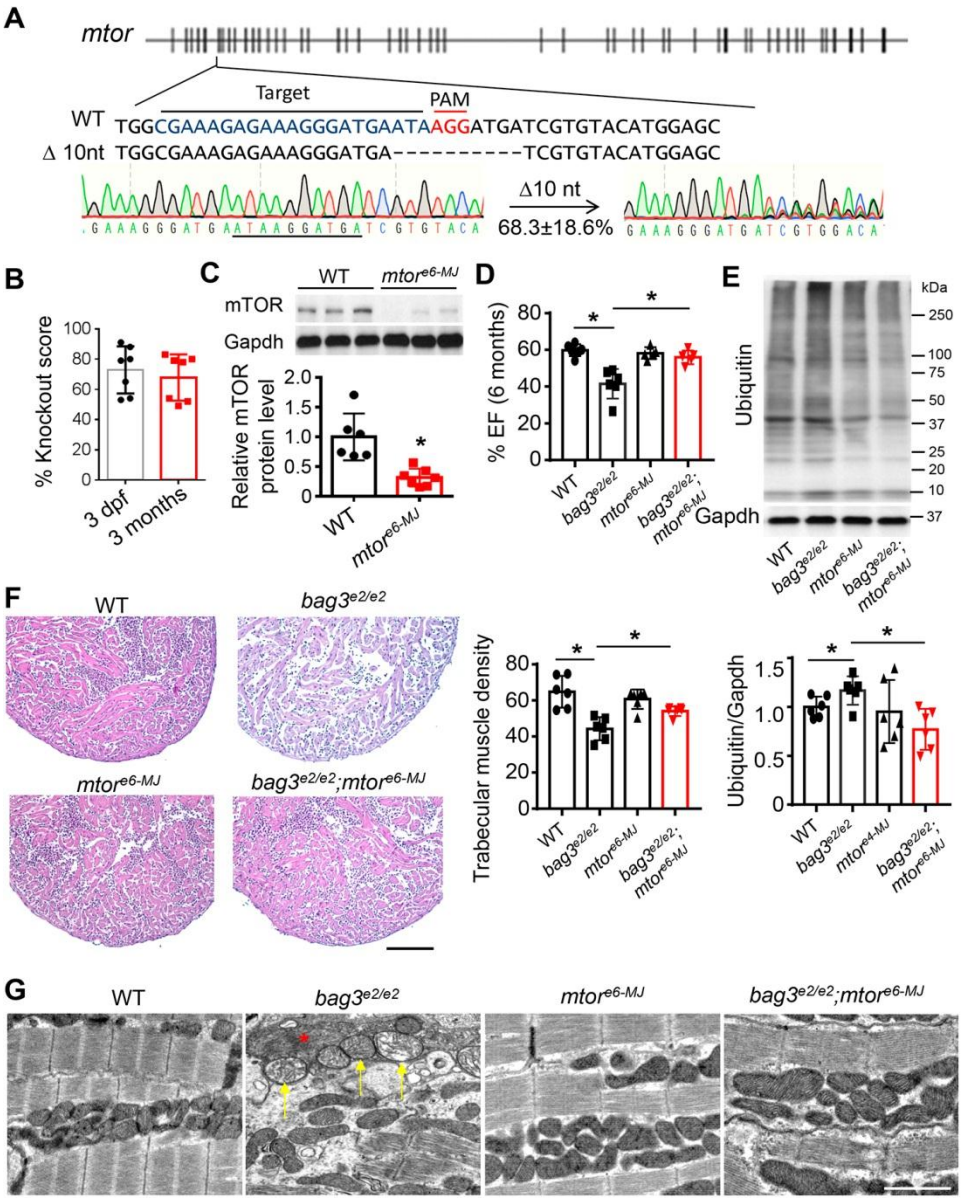

Fig. 3. The predicted MMEJ-inducing *mtor*-sgRNA injection exerted salutary modifier effects on *bag3* cardiomyopathy at F0

A, Design of the predicted MMEJ-inducing sgRNA sequence targeted to the sixth exon of *mtor* gene (*mtor*$^{e6\text{-}MJ}$). Injection of the *mtor*$^{e6\text{-}MJ}$ sgRNA led to generation of frame-shift mutant alleles with 68.3% predicted to result from microhomology recombination (a 10-nucleotide deletion). **B,**

Disease Models & Mechanisms • DMM • Accepted manuscript

The *mtor* gene KO score in the *mtor*$^{e6\text{-}MJ}$ injected fish embryos at 3 dpf. **C,** Western blot and quantification analysis of mTOR protein in the *mtor*$^{e6\text{-}MJ}$ fish compared to uninjected WT controls at 3 dpf. N=6, one way-ANOVA. **D,** EF of *the mtor*$^{e6\text{-}MJ}$ injected *bag3*$^{e2/e2}$ fish (*mtor*$^{e6\text{-}MJ}$;*bag3*$^{e2/e2}$) compared to *bag3*$^{e2/e2}$ mutant alone, *mtor*$^{e6\text{-}MJ}$ and uninjected WT controls at 6 months. N=6, one-way ANOVA. **E,** Western blot and quantification analysis of ubiquitinated protein level in the *mtor*$^{e6\text{-}MJ}$ injected *bag3*$^{e2/e2}$ fish hearts compared to uninjected controls at 6 months. N=6, one-way ANOVA. **F,** Representative H&E staining images from the apex area and quantification of the trabecular muscle density from the *mtor*$^{e6\text{-}MJ}$;*bag3*$^{e2/e2}$ fish compared to corresponding controls at 6 months. N=6, one-way ANOVA. Scale bar, 100 μM**. G,** Confirmative TEM images of *mtor*$^{e6\text{-}MJ}$ injected *bag3*$^{e2/e2}$ fish hearts compared to corresponding controls demonstrated largely restored mitochondrial swelling (arrows) and myofibril degeneration (star) phenotypes in the *mtor*$^{e6\text{-}MJ}$ injected *bag3*$^{e2/e2}$ fish at 6 months. Scale bar, 2 μM. *, P<0.05.

Disease Models & Mechanisms • DMM • Accepted manuscript

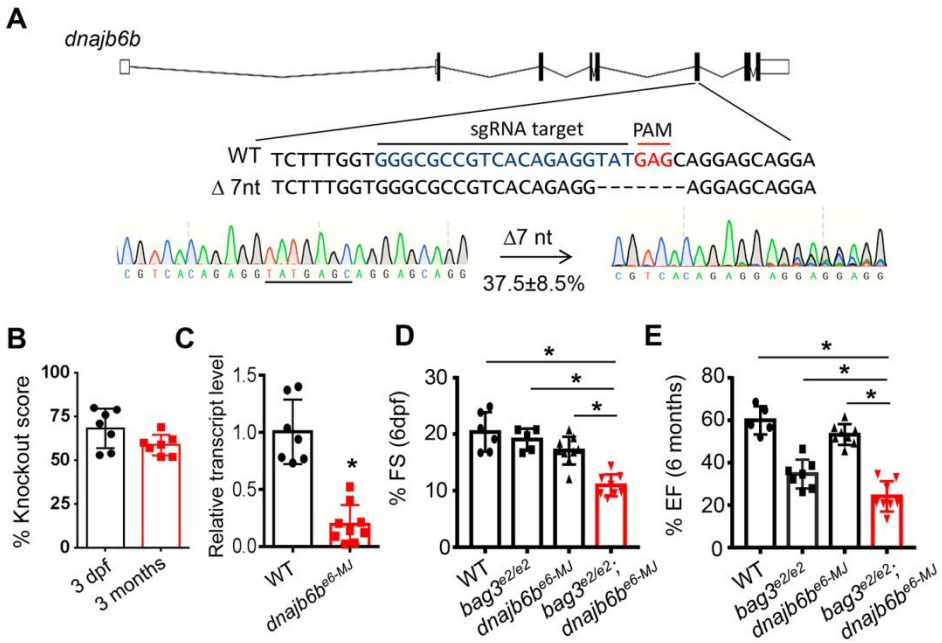

Fig. 4 . The predicted MMEJ-inducing *dnajb6b*-sgRNA injected *bag3*$^{e2/e2}$ F0 fish manifested severe cardiac dysfuntion

A, Design of the predicted MMEJ-based sgRNA sequence targeted to the sixth exon of *dnajb6b* gene (*dnajb6b*$^{e6\text{-}MJ}$). Injection of *dnajb6b*$^{e6\text{-}MJ}$ led to generation of frame-shift mutant alleles with 37.5% predicted to result from microhomology recombination (a 7-nucleotide deletion). **B,** The *dnajb6b* gene knockout (KO) scores in the *dnajb6b*$^{e6\text{-}MJ}$ injected fish at 3 dpf and 3 months. **C,** Transcript levels of the *dnajb6b* gene in the *dnajb6b*$^{e6\text{-}MJ}$ injected fish hearts compared to uninjected controls at 3 months. N=10. Unpaired student *t* test. **D-E,** FS (D) and EF (E) of the *dnajb6b*$^{e6\text{-}MJ}$ injected *bag3*$^{e2/e2}$ fish (*dnajb6b*$^{e6\text{-}MJ}$;*bag3*$^{e2/e2}$) compared to *bag3*$^{e2/e2}$ mutant alone, *dnajb6b*$^{e6\text{-}MJ}$ or uninjected WT controls at 6 dpf (embryonic) and 6 months (adult). Arrows point to accumulated lipid droplets. N=5-8, one-way ANOVA.

Disease Models & Mechanisms • DMM • Accepted manuscript

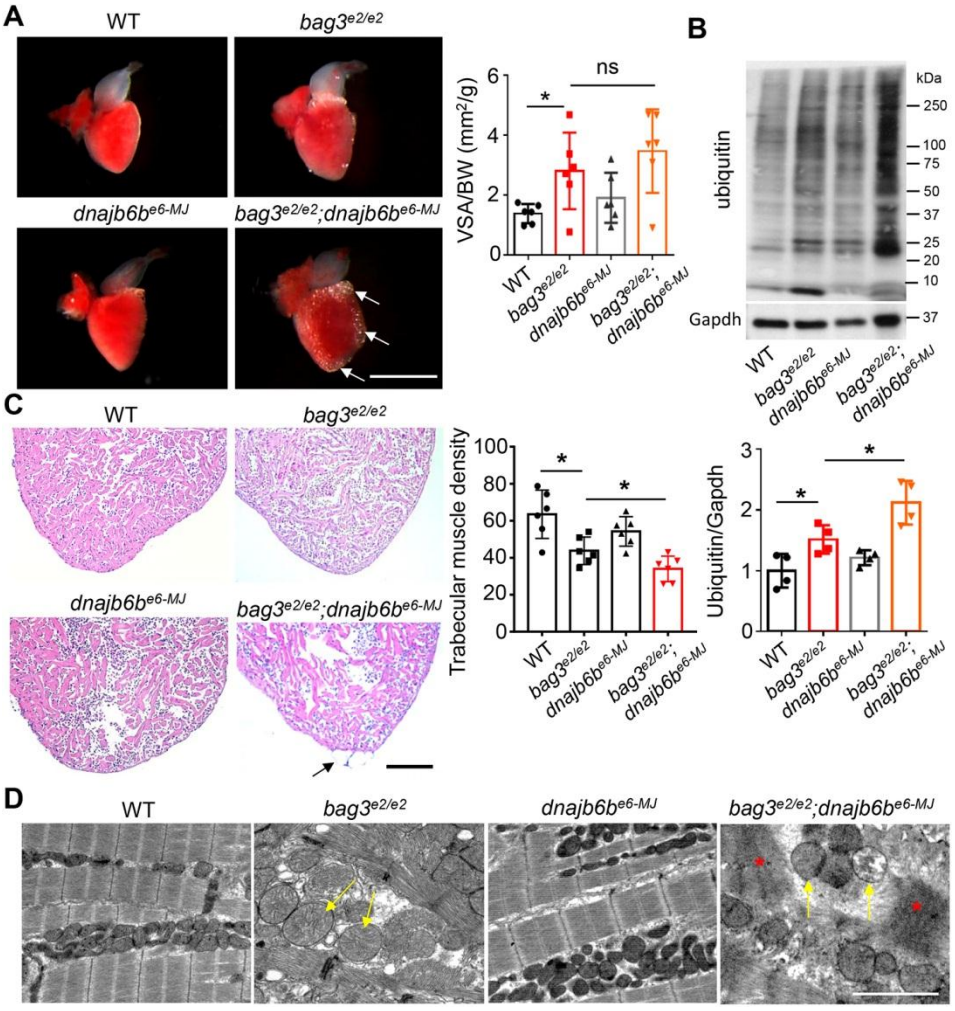

Fig. 5. The predicted MMEJ-inducing *dnajb6b*-sgRNA injected *bag3*$^{e2/e2}$ F0 adult fish manifested several phenotypic traits in the *bag3*$^{e2/+}$;*dnajb6b*$^{-/-}$ double stable mutants

A, The *dnajb6b*$^{e6\text{-}MJ}$;*bag3*$^{e2/e2}$ fish exhibited enlarged VSA/BW and lipid accumulation phenotypes. N=6, one-way ANOVA. Scale bar: 1 mm. **B,** Western blot and quantification analysis of ubiquitinated protein levels in the *dnajb6b*$^{e6\text{-}MJ}$;*bag3*$^{e2/e2}$ fish hearts compared to *bag3*$^{e2/e2}$ mutant alone, *dnajb6b*$^{e6\text{-}MJ}$ or uninjected WT controls at 6 months. N=4, one-way ANOVA. **C,** Representative H&E staining images from the apex area and quantification of the trabecular muscle density in the *dnajb6b*$^{e6\text{-}MJ}$;*bag3*$^{e2/e2}$ fish hearts compared to corresponding

Disease Models & Mechanisms • DMM • Accepted manuscript

controls at 6 months. The arrow points to lipid droplets. N=6, one-way ANOVA. Scale bar, 100 µM. **D,** Confirmative TEM images of *dnajb6b*$^{e6\text{-}MJ}$;*bag3*$^{e2/e2}$ fish hearts compared to corresponding controls demonstrated severe mitochondrial swelling (arrows) and myofibril degeneration (stars) phenotypes which are similar to those detected in the *bag3*$^{e2/+}$;*dnajb6b*$^{-/-}$ double mutant fish hearts**.** Scale bar, 2 µM. *, P<0.05. ns, not significant.

Disease Models & Mechanisms • DMM • Accepted manuscript

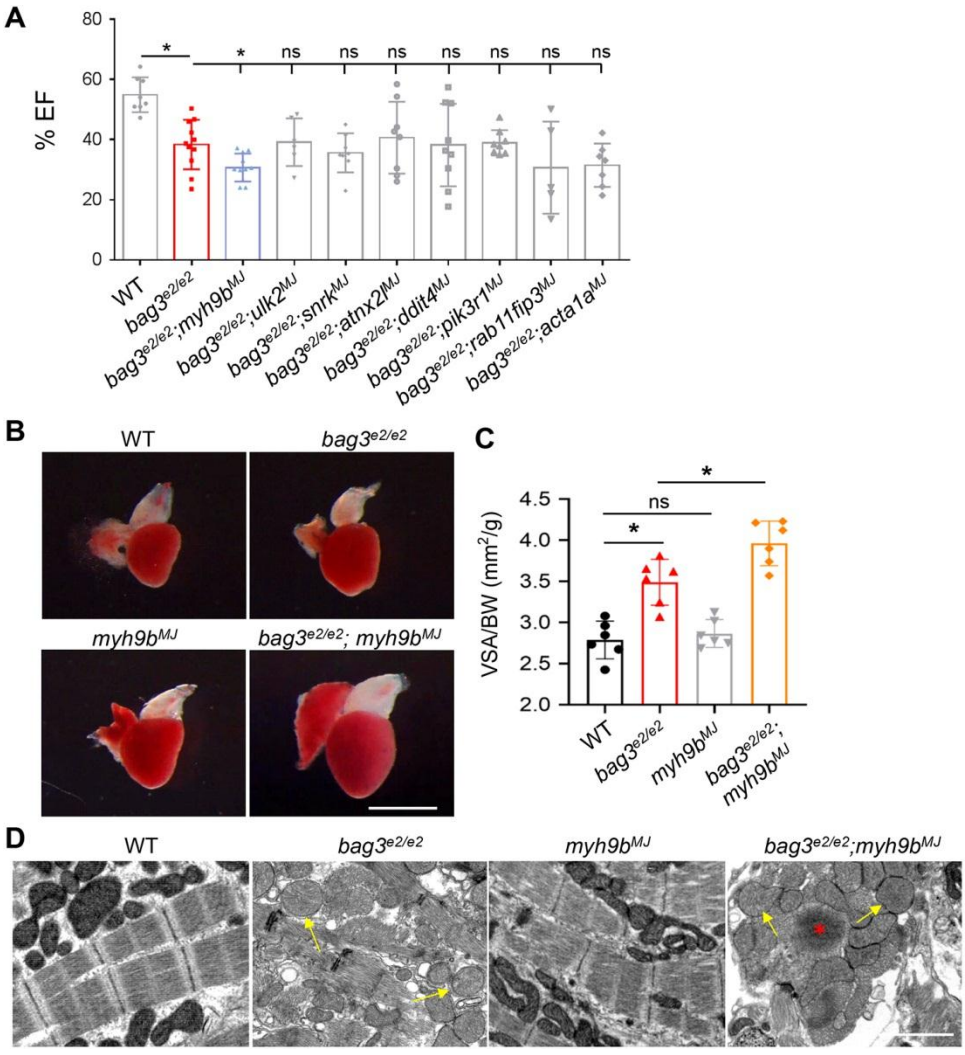

Fig. 6. identification of *myh9b* as a new deleterious modifier gene for *bag3* cardiomyopathy through predicted MMEJ-based genome editing at F0

A, EF of *bag3*$^{e2/e2}$ fish after injected with each of the 8 predicted MMEJ-based sgRNAs targeted to 8 differentially expressed (DE) proteostasis/autophagy genes compared to the *bag3*$^{e2/e2}$ single mutants and WT controls at 6 months. N=4-11, one-way ANOVA. B-**C,** The *myh9b*^{MJ} injected *bag3*$^{e2/e2}$ fish (*bag3*$^{e2/e2}$;*myh9b*^{MJ}) exhibited enlarged VSA/BW compared to the *bag3*$^{e2/e2}$ mutant alone, *myh9b*^{MJ} or uninjected WT controls at 6 months. N=6, one-way ANOVA. Scale

Disease Models & Mechanisms • DMM • Accepted manuscript

bar, 1 mm. **D,** Confirmative TEM images of the *bag3*$^{e2/e2}$; *myh9b*^{MJ} fish hearts compared to the *bag3*$^{e2/e2}$ mutant alone, *myh9b*^{MJ} or uninjected WT controls at 6 months. Arrows point swelling mitochondrial. Star indicates to sarcomeric Z-disc aggregation. Scale bar, 2 µM. *, P<0.05. ns, not significant.

Disease Models & Mechanisms • DMM • Accepted manuscript

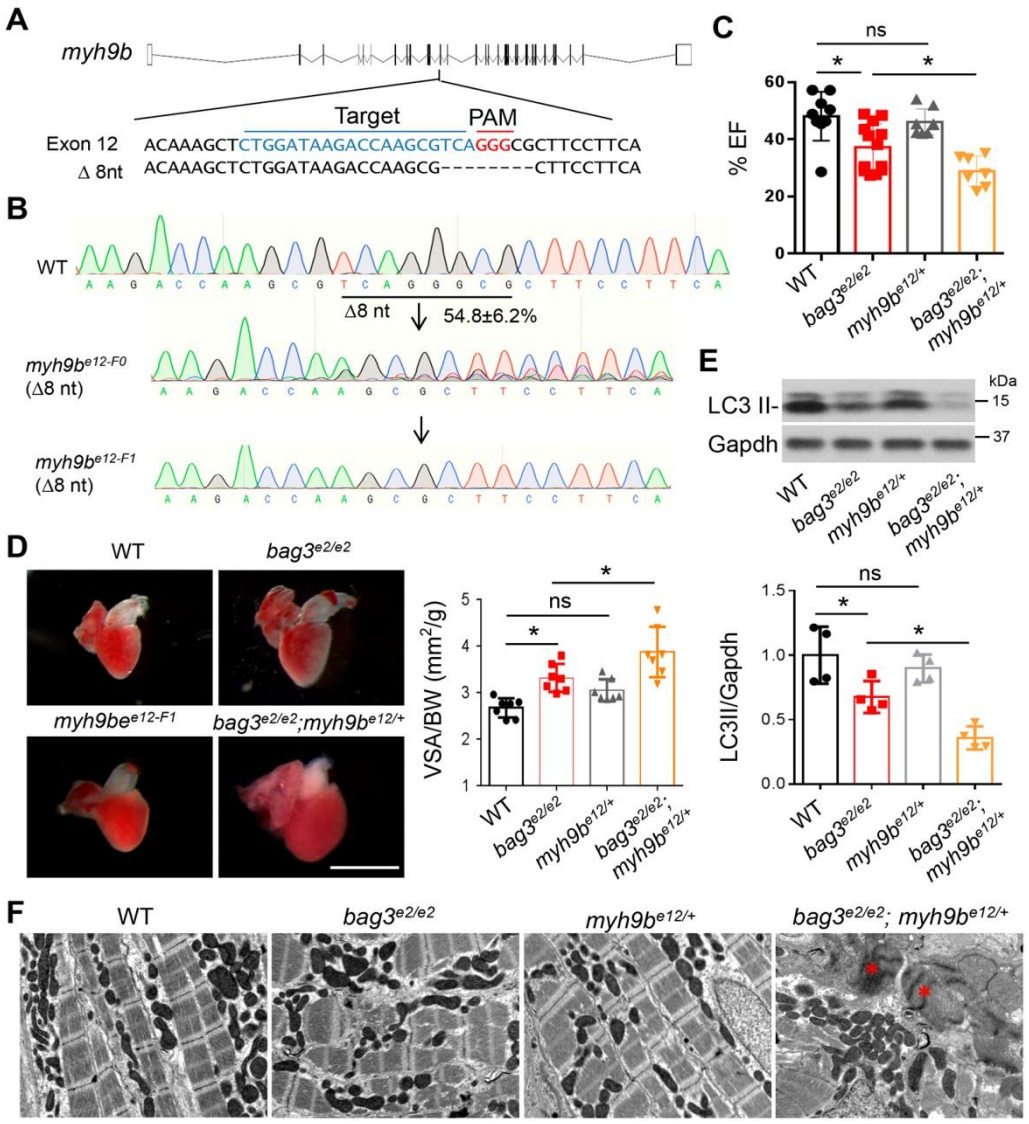

Fig. 7. The *myh9b* heterozygous stable mutant deteriorated *bag3* cardiomyopathy at adult stage

A, Schematics of predicted MMEJ-inducing *myh9b* genetic lesion of 8-nucleotide generated by injection of a sgRNA targeting at sequences in the 12nd exon. Dashed lines indicate a 8-nucleotide deletion. **B,** Chromographs illustrating the sequences of the wild-type *myh9b* sequence and the mutant alleles with the predicted 8-nucleotide deletion in F0 and F1 fish. **C,**

Disease Models & Mechanisms • DMM • Accepted manuscript

Quantification of cardiac function indices of percent ejection fraction (EF) measured using echocardiography in the *bag3*$^{e2/e2}$;*myh9b*$^{e12/+}$ double mutant fish compared to single mutants and WT control at 6 months. N=7-11, one-way ANOVA. **D,** Representative images of isolated hearts and quantification of the ventricular surface area (VSA) normalized to the body weight (BW) of fish at 6 months. N=7, one-way ANOVA. **E,** Western blot and quantification analysis of LC3 II protein levels in the *bag3*$^{e2/e2}$; *myh9b*$^{e12/+}$ double mutant fish hearts, *bag3*$^{e2/e2}$, *myh9b*$^{e12/+}$ or WT controls at 6 months. N=4, one-way ANOVA. **F,** TEM images of the *bag3*$^{e2/e2}$; *myh9b*$^{e12/+}$ double mutant fish hearts, *bag3*$^{e2/e2}$, *myh9b*$^{e12/+}$ or WT controls at 6 months. Stars indicate Z-disc aggregation. Scale bar, 2 µM. *, *P*<0.05. ns, not significant.

Disease Models & Mechanisms • DMM • Accepted manuscript

Table 1. Eight experimentally confirmed DE genes were prioritized for predicted MMEJ-inducing sgRNA injection in the *bag*$^{e2/e2}$ cardiomyopathy model

Gene	Exon	sgRNA target sequence	Predicted deletion	Knockout score (%)	Microhomology rate (%)
myh9b	12	CTGGATAAGACCAAGCGTCAGGG	TCAGGGCG	67.5±6.2	54.8±6.2
ulk2	8	ATGATGCCAAAGCTGACCTGTGG	ACCTG	78.5±15.5	65.3±9.4
snrkb	2	TGTTGTGTTCTTCAGGCAGCAGG	CAGCAGG	44.3±27.0	49.8±17.4
atxn2l	10	AACAGCTCTCTGTCAGTCAGAGG	TCAG	84.8±7.4	74.4±7.1
ddit4	2	CTCCAGGATAAGCGCTTCGCTGG	CTTCG	74.7±7.8	93.9±3.3
pik3r1	2	CAGACTGTCAAGTGTGGATGGGG	ATGG	82.8±11.9	79.7±9.3
rab11fip3	4	GAAGATGTGGAGACAGACAGCGG	ACAG	82.8±5.1	80.4±8.8
acta1a	3	CAACGTCCCCGCTATGTATGTGG	ATGG	67.5±6.2	54.8±6.2

Disease Models & Mechanisms • DMM • Accepted manuscript

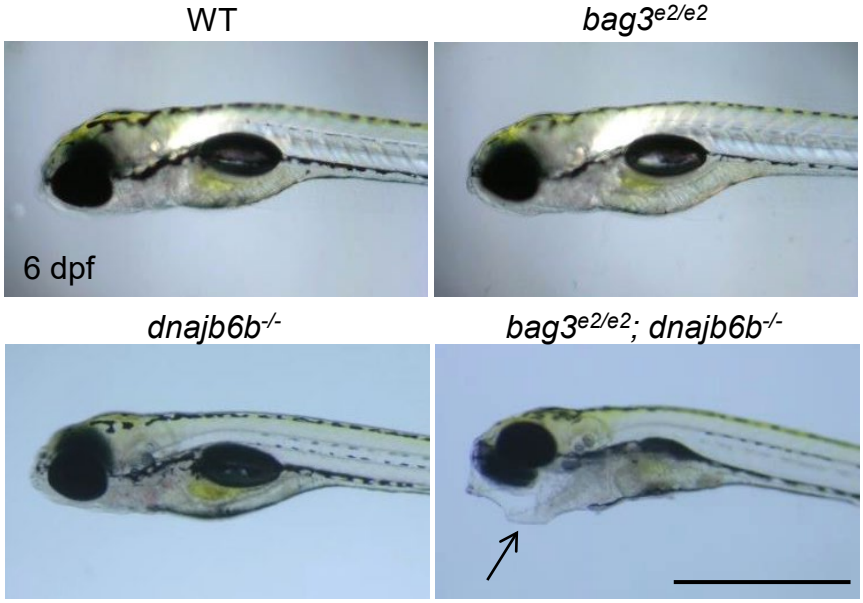

Fig. S1. The homozygous *GBT411/dnajb6b* mutant exerted deleterious effects on the *bag3*$^{e2/e2}$ mutant

Images of the *bag3*$^{e2/e2}$*; dnajb6b*$^{-/-}$ double mutant fish compared to the *bag3*$^{e2/e2}$ or *dnajb6b*$^{-/-}$ single mutants and WT controls at 6 days post-fertilization (dpf). Scale bar, 1 mm.

Disease Models & Mechanisms • Supplementary information

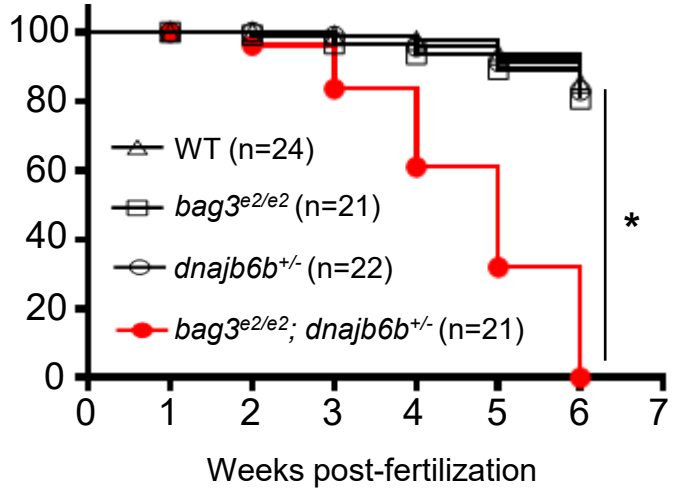

Fig. S2. The heterozygous G*BT411/dnajb6b* mutant exerted deleterious effects in survival on the *bag3*$^{e2/e2}$ mutant

Survival curves of *bag3*$^{e2/e2}$*; dnajb6b*$^{+/-}$ double mutant fish compared to single mutants and WT controls. * N=21-24. * *P*<0.05, Log rank test.

Disease Models & Mechanisms • Supplementary information

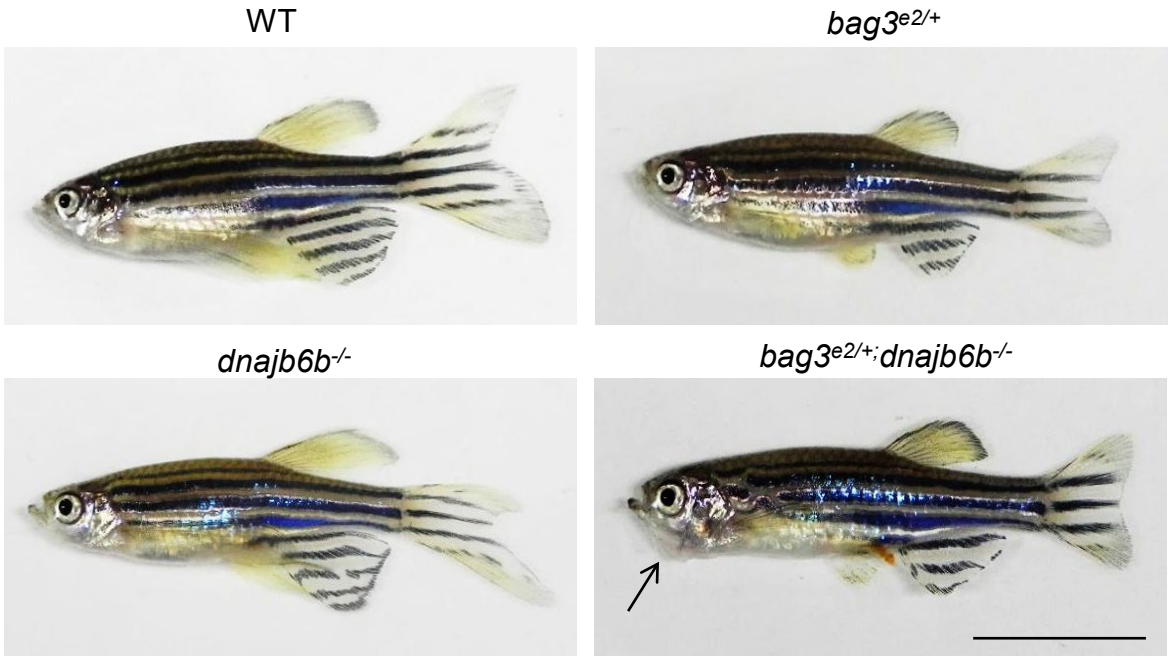

Fig. S3. Genetic interaction between *bag3*$^{e2/+}$ and *dnajb6b*$^{-/-}$ mutant fish Representative images of *bag3*$^{e2/+}$; *dnajb6b*$^{-/-}$ double mutant fish and their corresponding single mutant controls at 3 months of age. The arrow points to unusual jaw protruding phenotype. Scale bar: 1 cm.

Disease Models & Mechanisms • Supplementary information

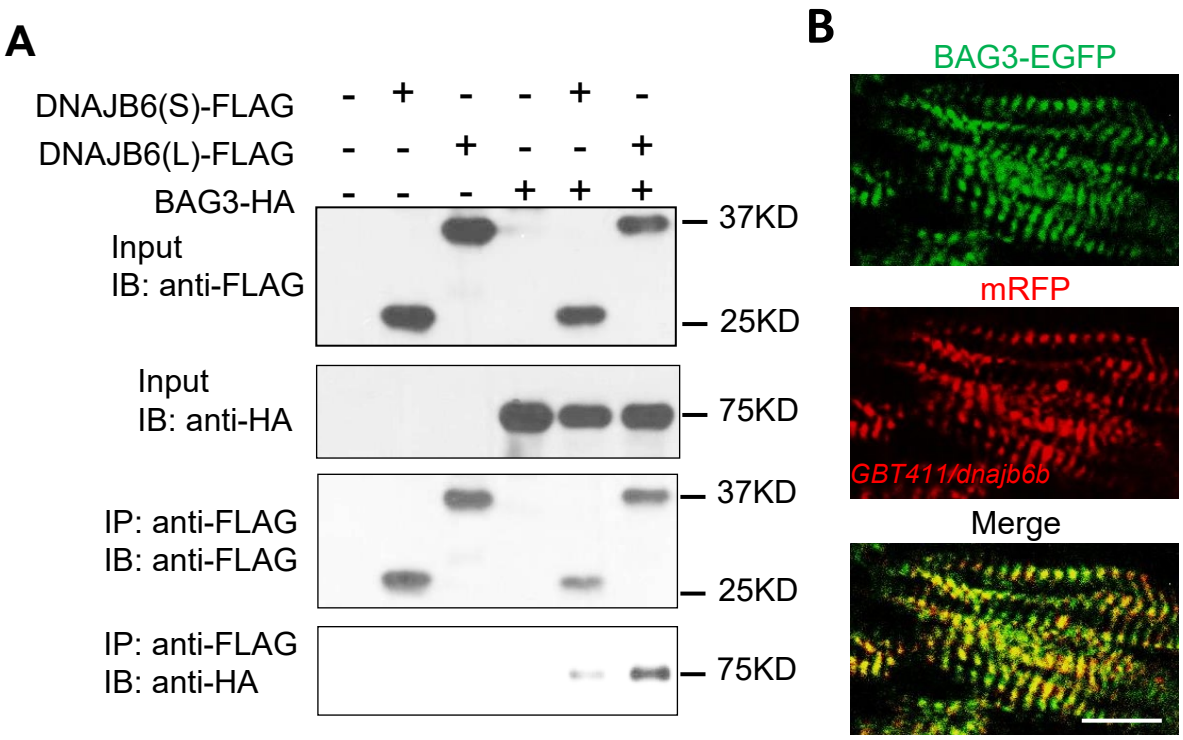

Fig. S4. DNAJB6 protein interacts with BAG3 *in vitro*

A, Western blot analysis of the *in vitro* protein pull-down assay indicated a direct protein-protein interaction between the human DNAJB6(L) and BAG3 proteins and between the human DNAJB6(S) and BAG3 proteins in the HEK293 cells. IP: immunoprecipitation. IB: immunoblot. **B**, Fluorescent images of adult heart sections from *GBT411/dnajb6b* mutant after crossed with the *Tg(cmlc2:BAG3-EGFP)* transgenic fish. Scale bar, 10 μm.

Disease Models & Mechanisms • Supplementary information

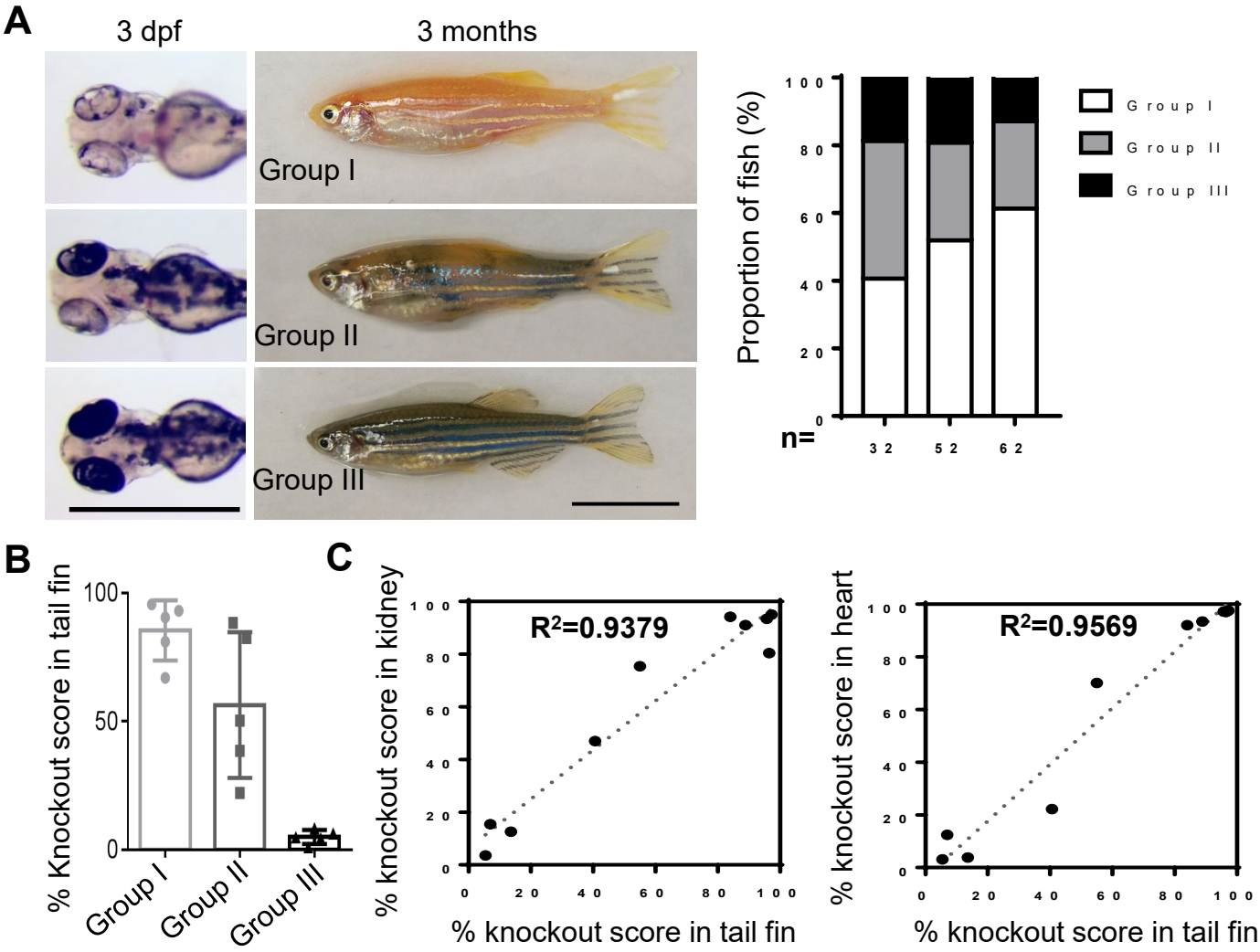

Fig. S5. Effective gene knockout by microhomology-mediated end-joining (MMEJ)-based *tyrosin* single guide RNA sustained from embryonic to adult stages

A-B, Representative images and quantification of *tyrosine* (*tyr*) microhomology-mediated end-joining (MMEJ)-based single guide RNA (sgRNA) injected fish at 3 dpf and 3 months categorized from high to low knockout (KO) score (group I to group III). Scale bar in left panels, 1mm, right panels, 1 cm. Three bars in the bar graph in (**A**) represent results from three independent injections of *tyr* sgRNA. **C,** Correlation of KD score calculated using genomic DNA extracted from the tail fin, heart or kidney, respectively.

Disease Models & Mechanisms • Supplementary information

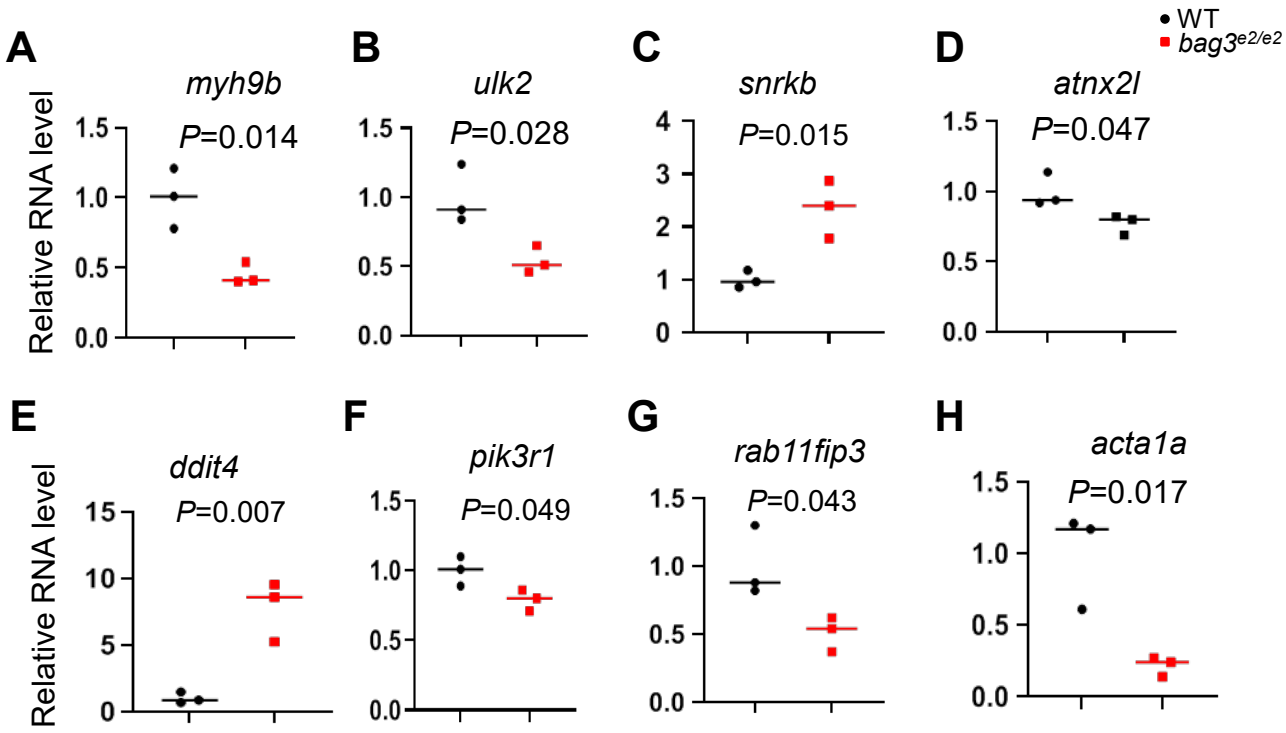

Fig. S6. Quantitative RT-PCR results of 8 differentially expressed proteostasis/autophagy genes in the *bag*$^{e2/e2}$ cardiomyopathy model

Disease Models & Mechanisms • Supplementary information

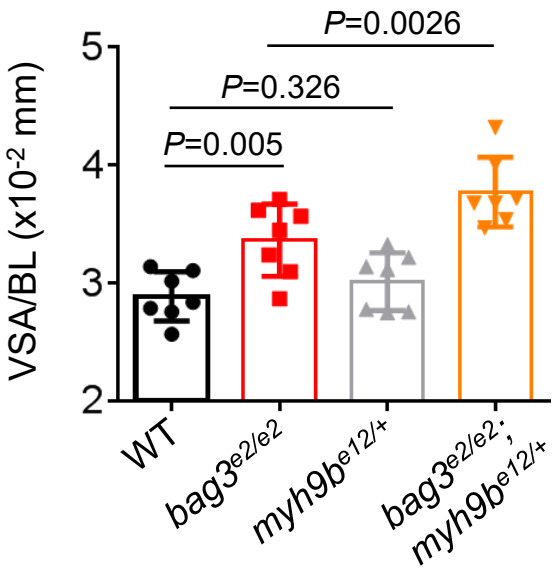

Fig. S7. *The bag3$^{e2/e2}$;myh9b$^{e12/+}$* double mutant fish displayed enlarged ventricular chamber size

Quantification of the ventricular surface area (VSA) normalized to the body length (BL) of fish at 6 months. N=6, one-way ANOVA.

Disease Models & Mechanisms • Supplementary information

Table S1. Primers for genotyping PCR to identify the *bag3*$^{e2/e2}$ and gene-break transposon (GBT) mutants

Primer name	Primer Sequence
RP2-5'-LTR	5'-GCATGAACTCCTTGATGACG-3'
RP2-3'-LTR	5'-GTACAGTAATCAAGTAAAATTACTCA-3'
GBT002/sorbs2b-F	5'-GGGTCGGCATGCTTCATCACTG-3'
GBT002/sorbs2b-R	5'-AATCCAGCAGACCGAACAAACGC-3'
GBT136/ano5a-F	5'-AGGGTCTTTGTGGATGTCTGTGAATG-3'
GBT136/ano5a-R	5'-CTGAGGTCTCTGCACAACCTATTAGTGT-3'
GBT411/dnajb6b-F	5'-TGTGATAACATCACAGCACC-3'
GBT411/dnajb6b-R	5'-ACGATGAAAATGAGCTGAAGC-3'
GBT419/rxraa-F	5'-ATATCGCTTTAGTTCGCTCACTTTAT-3'
GBT419/rxraa-R	5'-TATATACACGAAAATCCTCCACACA-3'
bag3-F	5′-CGGCGTATAAAGAATTGCTGG-3'
bag3-R	5′-GTGAAGTAGGTGAGCAAGAC-3'

Disease Models & Mechanisms • Supplementary information

Table S2. Quantitative RT-PCR primers used to validate differentially expressed (DE) genes

Gene	Primer Sequence
acta1a	F: 5'-CAGCTTTACTTCAGGACTCACG-3'
	R: 5'-TACCTCTCTTGCTCTGAGCCTC-3'
ddit4	F: 5'-AGCCATCAGACTTGAGGATAC-3'
	R: 5'-GGGTCGAAAAACTCAGATTGG-3'
atnx2l	F: 5'-ACCCGAGACACTTTCACAG-3'
	R: 5'-GACTGGAGTCATAGGTGGAC-3'
pik3r1	F: 5'-AACTCCTAAACCGAGACCTC-3'
	R: 5'-AGCACTGTCTGACATCCAG-3'
snrkb	F: 5'-CGG ACGCATGAAGATTTCAG-3'
	R: 5'- CATATAGACCAGCTATCTTGCC-3'
ulk2	F: 5'-AAGACTGATTGGGAGGTCG-3'
	R: 5'- GCTGCAATCTGCTGTAGAAAG-3'
myh9b	F: 5'-ATCTACTCAGAGGAGATCGTG-3'
	R: 5'- GCTGCTCTGGTCTTTCTTG-3'
rab11fip3	F: 5'-AGGCATCAGTGCAATCAGC-3'
	R: 5'-GTCGTCTCCATCTGTGAGT-3'

Disease Models & Mechanisms • Supplementary information

Table S3. PCR primers for quantifying knockout efficiency of predicted MMEJ-inducing sgRNAs

Gene	Primer Sequence
atxn2l	F: 5'-CCTGCCTAATCGAACAAATCG-3'
	R: 5'-GTGTGAGAGTGAATGTGAGAG-3'
myh9b	F: 5'-GAATGTGACCGATTTCACCC-3'
	R: 5'-CCTCAAAGATCTCAAAGCCG-3'
ulk2	F: 5'-CTGAAGGCTGTCTCAGATTG-3'
	R: 5'-ACTTTAGGCATTCAACCGTAG-3'
snrkb	F: 5'-CGGACGCATGAAGATTTCAG-3'
	R: 5'-CATATAGACCAGCTATCTTGCC-3'
rab11fip3	F: 5'-AGGCATCAGTGCAATCAGC-3'
	R: 5'-GTCGTCTCCATCTGTGAGTG-3'
pik3r1	F: 5'-AACTCCTAAACCGAGACCTC-3'
	R: 5'-AGCACTGTCTGACATCCAG-3'
ddit4	F: 5'-GATAACTGATCATGCAGGACTG-3'
	R: 5'-TGCACACCTGAATCTGAGG-3'
acta1a	F: 5'-CACCACACCTTCTACAATGAG-3'
	R: 5'-ACATCAGAGTTTTCGATCAGC-3'
dnajb6b	F: 5'-CACAGTGAGCCTGAAATGATG-3'
	R: 5'-AGCTGCACACAGATTAACATAC-3'
mtor	F: 5'-AGGTGCAGCCATTCTTTGAT-3'
	R: 5'-ATGTCATACCTCTCCCTCCATAC-3'
tryosinase	F: 5'-GCGTCTCACTCTCCTCGACTCTTC-3'
	R: 5'-GTAGTTTCCGGCGCACTGGCAG-3'

Disease Models & Mechanisms • Supplementary information